Article

Molecular Cell

A Conserved Kinase-Based Body-Temperature Sensor Globally Controls Alternative Splicing and Gene Expression

Graphical Abstract

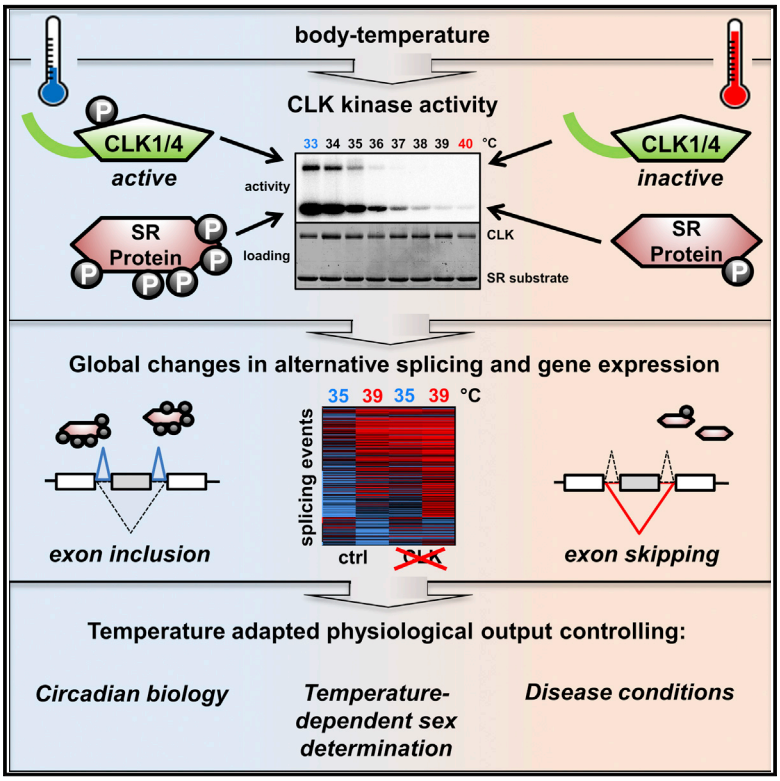

Highlights

- CLK kinases are thermo-sensors reactive to subtle body-temperature changes
- Body temperature globally controls splicing and gene expression through CLKs
- CLK homologs are evolutionarily adapted to diverse body/growth temperatures
- Wide functionality of CLKs: from TSD in reptiles to circadian biology in mammals

Authors

Tom Haltenhof, Ana Kotte, Francesca De Bortoli, ..., Markus C. Wahl, Marco Preußner, Florian Heyd

Correspondence

florian.heyd@fu-berlin.de

In Brief

Haltenhof et al. show that the activity of CLK kinases is extremely sensitive to physiological temperature changes. This cellular thermometer is based on minor structural rearrangements of the kinase activation segment, representing a new concept in enzymology. CLKs globally control alternative splicing and gene expression in a (body) temperature-dependent manner, with wide implications ranging from circadian biology to disease conditions. This thermometer is evolutionarily adapted to the growth temperature of diverse organisms with implications for reptilian temperature dependent sex determination.

Haltenhof et al., 2020, Molecular Cell *78*, 57–69
April 2, 2020
https://doi.org/10.1016/j.molcel.2020.01.028

CellPress

Molecular Cell
Article

A Conserved Kinase-Based Body-Temperature Sensor Globally Controls Alternative Splicing and Gene Expression

Tom Haltenhof,[1] Ana Kotte,[1] Francesca De Bortoli,[1] Samira Schiefer,[1] Stefan Meinke,[1] Ann-Kathrin Emmerichs,[1] Kristina Katrin Petermann,[1] Bernd Timmermann,[2] Petra Imhof,[3] Andreas Franz,[1,4] Bernhard Loll,[4] Markus C. Wahl,[4,5] Marco Preußner,[1] and Florian Heyd[1,6,*]

[1]Freie Universität Berlin, Institute of Chemistry and Biochemistry, Laboratory of RNA Biochemistry, Takustrasse 6, 14195 Berlin, Germany
[2]Sequencing Core Facility, Max-Planck-Institute for Molecular Genetics, Ihnestraße 63-73, Berlin 14195, Germany
[3]Freie Universität Berlin, Institute of Theoretical Physics, Arnimallee 14, 14195 Berlin, Germany
[4]Freie Universität Berlin, Institute of Chemistry and Biochemistry, Laboratory of Structural Biochemistry, Takustrasse 6, 14195 Berlin, Germany
[5]Helmholtz-Zentrum Berlin für Materialien und Energie, Macromolecular Crystallography, Albert-Einstein-Straße 15, 12489 Berlin, Germany
[6]Lead Contact
*Correspondence: florian.heyd@fu-berlin.de
https://doi.org/10.1016/j.molcel.2020.01.028

SUMMARY

Homeothermic organisms maintain their core body temperature in a narrow, tightly controlled range. Whether and how subtle circadian oscillations or disease-associated changes in core body temperature are sensed and integrated in gene expression programs remain elusive. Furthermore, a thermo-sensor capable of sensing the small temperature differentials leading to temperature-dependent sex determination (TSD) in poikilothermic reptiles has not been identified. Here, we show that the activity of CDC-like kinases (CLKs) is highly responsive to physiological temperature changes, which is conferred by structural rearrangements within the kinase activation segment. Lower body temperature activates CLKs resulting in strongly increased phosphorylation of SR proteins *in vitro* and *in vivo*. This globally controls temperature-dependent alternative splicing and gene expression, with wide implications in circadian, tissue-specific, and disease-associated settings. This temperature sensor is conserved across evolution and adapted to growth temperatures of diverse poikilotherms. The dynamic temperature range of reptilian CLK homologs suggests a role in TSD.

INTRODUCTION

The environmental temperature has a strong influence on all three domains of life. Examples include daily changes in temperature that serve as Zeitgeber ("time giver") for the circadian clock, seasonal changes in temperature that are linked to hibernation and temperature-dependent sex determination in some reptiles (Buhr et al., 2010; Capel, 2017). In addition, sensing cold and hot temperatures is essential to avoid extreme and potentially dangerous conditions. Therefore, diverse organisms, including humans, have evolved complex thermosensory systems (Tan and Katsanis, 2009). With respect to cold sensing in mammals, two receptors were identified that react to cool (below 26°C) or cold (below 20°C) external temperature, namely, Trpm8 and GluK2 (Bautista et al., 2007; Gong et al., 2019). On the other hand, several members of the TRP family have been reported to respond to warm or hot temperature (43°C or above; Wetsel, 2011). TRP channels sense changes in environmental temperature, and their function is therefore best characterized in skin and primary sensory neurons (Wetsel, 2011). In contrast to the body shell, the core body temperature in homeothermic organisms is largely independent of the external temperature and kept within a narrow range. Most organs and cells are therefore not exposed to strong ambient temperature changes but rather experience subtle changes in core body temperature. For example, most mammals display a body temperature of around 37°C that shows circadian (~24-h) oscillation within a range of ~1°C–4°C (Buhr et al., 2010; Refinetti and Menaker, 1992; Saini et al., 2012). The female hormone cycle and aging also have a mild effect on core body temperature, as have pathological conditions such as hypothermia, fever, or the slightly increased temperature in tumor tissue (Charkoudian et al., 2017; Gautherie and Gros, 1980; Keil et al., 2015). The cellular cold and heat shock responses are triggered below 35°C and above 39°C, respectively, and many studies have used even more extreme and unphysiological temperatures, typically 32°C and 42°C, to elicit a full response. Therefore, whether and how cells are able to sense and respond to subtle changes in the physiologically relevant range of the core body temperature remain unknown.

Our recent finding that a 1°C–2°C oscillation of body temperature is sufficient to control alternative splicing (AS) (Preußner et al., 2017) implies the presence of a cellular thermometer that is able to sense very subtle, endogenous changes in the physiological temperature range. Rhythmic AS is regulated through altered phosphorylation of the serine arginine (SR)-rich domain

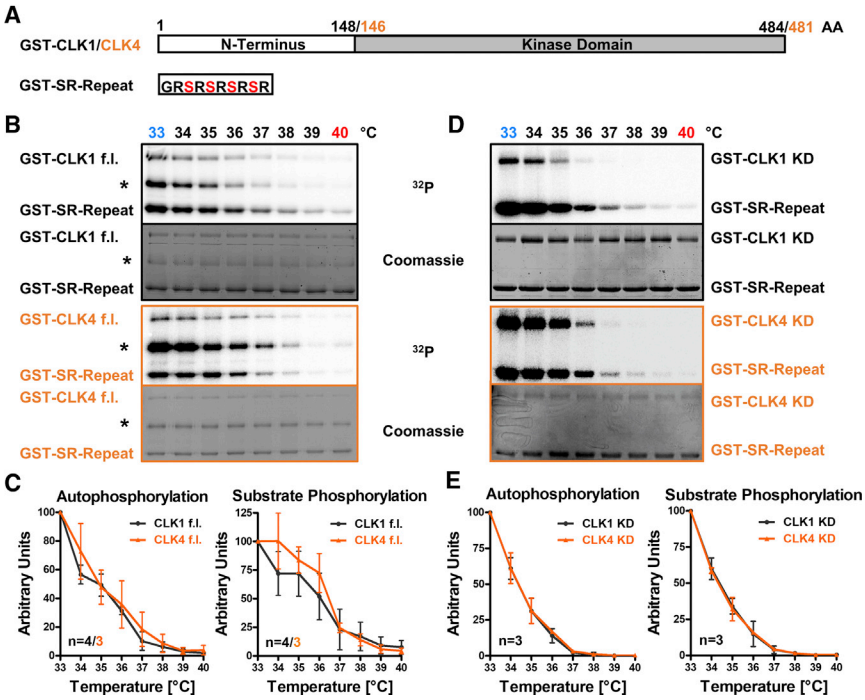

Figure 1. The Activity of the CLK1/4 Kinase Domain Is Controlled by Changes in the Physiologically Relevant Temperature Range

(A) Schematics of mouse CLK1/4 kinases and a serine/arginine (SR) peptide substrate. Borders in CLK1 and CLK4 domain organization are highlighted in black (CLK1) or orange (CLK4), respectively.

(B) An *in vitro* kinase assay with f.l. kinases. GST-tagged CLK1 (top, black) and CLK4 (bottom, orange) were purified from bacteria and coupled to glutathione beads, incubated with GST-SR and ^{32}P-γ-ATP at the indicated temperatures. After SDS-PAGE, phosphorylation was investigated by autoradiography (top, ^{32}P), and equal loading was confirmed by Coomassie staining (bottom). The asterisks most likely represent extended kinase domains, which lost the GST tag due to cleavage in the unstructured N termini by residual proteases, and which are also phosphorylated in a temperature-dependent manner.

(C) Quantification of auto- and substrate phosphorylation experiments as in (B) relative to the highest activity (n = 3 for CLK4, n = 4 for CLK1).

(D) *In vitro* kinase assays as in (B) with purified kinase domains (KD).

(E) Quantification of experiments as in (D) (n = 3).

In (C) and (E), data represent means ± standard deviations (SDs). See also Figure S1.

of SR proteins, with higher phosphorylation levels at lower body temperature. SR proteins are splicing-activating RNA binding proteins and their phosphorylation is controlled by two classes of kinases, SRPKs (SR protein kinases, SRPK1–3) and CLKs (CLK1–4) (Dominguez et al., 2016; Ghosh and Adams, 2011). SRPKs phosphorylate SR proteins in the cytoplasm triggering nuclear import and localization in speckles (Zhou and Fu, 2013). Further nuclear phosphorylation by CLKs mobilizes SR proteins (Aubol et al., 2016; Colwill et al., 1996), which then control transcription and all further (pre-)mRNA processing events, from splicing, to nuclear export, translation, and degradation (Long and Caceres, 2009; Müller-McNicoll et al., 2016). Knockdown and inhibitor experiments suggested an involvement of the close homologs CLK1 and CLK4 in the temperature-dependent control of SR protein phosphorylation (Preußner et al., 2017). Although so far no enzymes have been described whose activity substantially changes within the narrow range of core body temperature, we hypothesized that this could be the case for CLK activity. This would define an additional class of cellular temperature sensors that are, in contrast to TRP channels that react mainly to changes in ambient temperature, able to sense changes in the internal body temperature.

In line with this hypothesis, we show here that body temperature controls the activities of CLKs, resulting in dramatically altered SR protein phosphorylation within the physiological temperature range. CLK activity is more than 5-fold higher at 35°C than at 38°C, which contradicts the Q_{10} rule and thus has to be actively regulated, and matches corresponding changes in endogenous SR protein phosphorylation (Preußner et al., 2017). We furthermore show a global impact of body-temperature changes on AS and gene expression in human cells, which is predominantly controlled by CLK activity. This includes identification of a CLK-dependent AS event in the cold-induced RNA-binding protein (CIRBP) regulating its cold-induced gene expression. We thus define a cellular thermo-sensor that integrates subtle changes in the endogenous core body temperature into gene expression programs. The extreme temperature sensitivity is based on reversible temperature-induced structural rearrangements in the activation segment, representing an inherent feature of the protein itself that does not require additional regulators, thus providing a paradigm-setting example for the regulation of enzymatic activity in the physiological temperature range. CLK temperature sensitivity is conserved across evolution and adapted to growth temperatures of diverse poikilotherms, which adapt their body temperature to the surrounding temperature. The dynamic temperature range of reptilian CLK homologs suggests a role as molecular thermometer in TSD.

RESULTS

CLK1/4 Activity Is Highly Responsive to Physiological Temperature Changes

While rhythmic AS of numerous exons is controlled by oscillating body temperature (Goldammer et al., 2018; Preußner et al., 2017; Preußner and Heyd, 2018), a temperature sensor that connects such small temperature changes with AS remains unknown. As rhythmic AS depends on body-temperature-controlled SR protein phosphorylation, we hypothesized that the activity of CLK kinases could be directly controlled by body temperature. To address a potential role of CLKs as molecular thermometers, we expressed and purified mouse GST-tagged CLK1 and CLK4 from bacteria (Figures 1A and S1A). Both

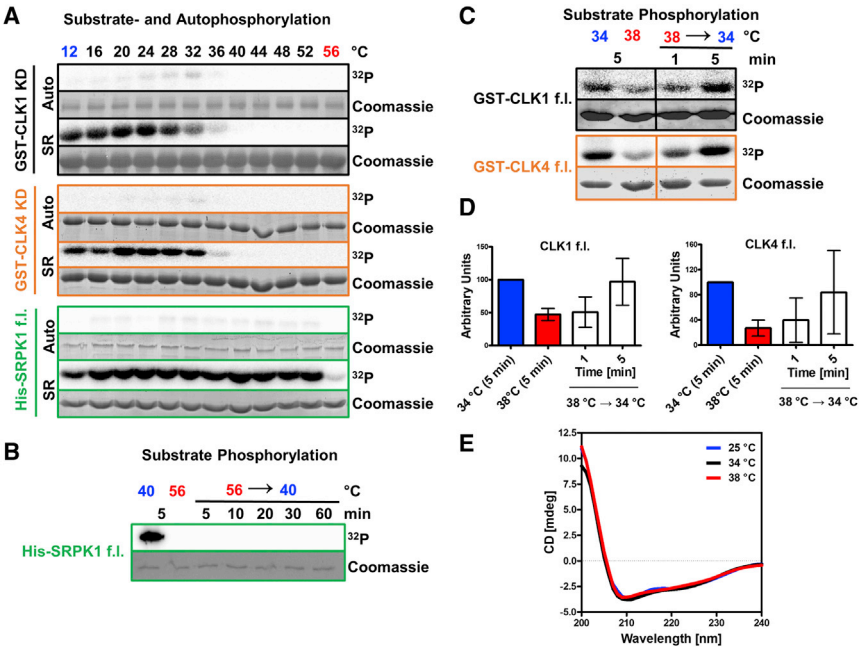

Figure 2. Temperature-Dependent SR Protein Phosphorylation Is Specifically Mediated by CLK1/4, and the Inactivation at High Temperature Is Reversible

(A) Kinase activity was investigated as in Figure 1B in an extended temperature range (indicated on top) for CLK1 (black), CLK4 (orange), and the SR protein kinase SRPK1 (green).

(B) Heat-induced inactivation of SRPK1 is irreversible. Substrate phosphorylation was investigated after incubation for 5 min at 56°C and then shifting the reactions back to 40°C for the indicated times.

(C and D) Reversible inactivation of CLK1/4. Substrate phosphorylation was investigated after incubation at 38°C and shifting the reactions back to 34°C for the indicated times. Quantifications of experiments as in (C) are shown in (D) (n = 3, mean ± SD).

(E) CD spectra of the CLK1 kinase domain at 25°C (blue), 34°C (black), and 38°C (red). Data represent the mean of three recorded spectra.

kinases are widely expressed across different tissues and show 91/97% homology to the human variants. We used purified CLK proteins in *in vitro* kinase assays with auto- and SR-repeat phosphorylation as readout. In a temperature gradient from 33°–40°C, we find the activity of both CLKs to be strongly temperature dependent with higher activity at lower temperature, matching the phosphorylation state of SR proteins *in vivo* (Preußner et al., 2017) (Figures 1B and 1C). In previous work, mouse CLK1 activity was assessed, e.g., at 37°C (Keshwani et al., 2015); the same study assayed human CLK1 at 23°C without explaining the different temperatures, and a temperature-dependent activity was not investigated. For both auto- and SR-repeat phosphorylation, we find CLK1/4 to be almost completely inactive at 38°C, whereas they show considerable activity at 35°C (50%–80% of the activity at 33°C), representing a more than 5-fold change (Figure 1C). This substantial change in activity occurred through a change of 3°C, between 35°C and 38°C, precisely in the range in which circadian body-temperature oscillations occur (Buhr et al., 2010; Preußner et al., 2017; Saini et al., 2012). As the *in vitro* kinase reactions contain only purified protein and substrate, temperature sensitivity is independent of additional interaction partners or posttranslational modifications, thus representing an inherent feature of the kinases itself.

CLKs consist of an unstructured N-terminal region and the C-terminal kinase domain (KD) (Ghosh and Adams, 2011) (Figure 1A). To investigate which part of the protein mediates temperature sensitivity, we purified the KDs alone. Mouse and human CLK1/4 KDs showed strong temperature dependence in both auto- and SR-peptide phosphorylation (mouse variants in Figures 1D and 1E; see Figure S1B for the human variants and comparison between mouse and human), showing that the CLK KD is itself temperature sensitive and that this feature is conserved across different mammals. However, as the activity profiles differ slightly between the full-length (f.l.) proteins and the KDs (Figure S1C), the precise temperature range is partially set by the unstructured N terminus. CLK-mediated phosphorylation is specific for the SR substrate, as GST alone is not phosphorylated, and is not affected by (potentially temperature-induced) differences in the pH between 6.9 and 7.6 (Figures S1D and S1E). For further experiments, we have used the respective KDs, as they recapitulate temperature sensitivity and can be produced as pure and stable proteins (Figures S1F–S1I).

Body-Temperature Sensitivity Is Specific for CLKs and Depends on Reversible Inactivation

To start addressing the molecular basis for higher CLK activity at lower temperatures and to investigate whether related kinases show a similar behavior, we purified a member of the other family of SR protein kinases, namely, SRPK1. We then compared temperature-activity profiles of CLKs and SRPK1 in a wider temperature range between 16°C and 56°C. As before, the activity of CLKs was strongly reduced between 32°C and 36°C, with CLK1 activity starting to decrease at 28°C already (Figure 2A). CLK1 thus appears to be optimized for temperatures below physiological levels, which may help to respond in suboptimal conditions where kinase activity could become limiting. In contrast to the CLKs, SRPK1 activity was constant between 16°C and 52°C with a loss of activity at 56°C, confirming that temperature sensitivity in the physiological temperature range is not a general feature of all protein kinases (Thomas and Scopes, 1998). The wide temperature range of almost unchanged SRPK1 activity is an interesting feature, suggesting that SRPK1 is intrinsically temperature compensated. The inactivation temperature of SRPK1 at 56°C is close to the median denaturing temperature of human proteins of ~60°C (Leuenberger et al., 2017), and loss of activity probably

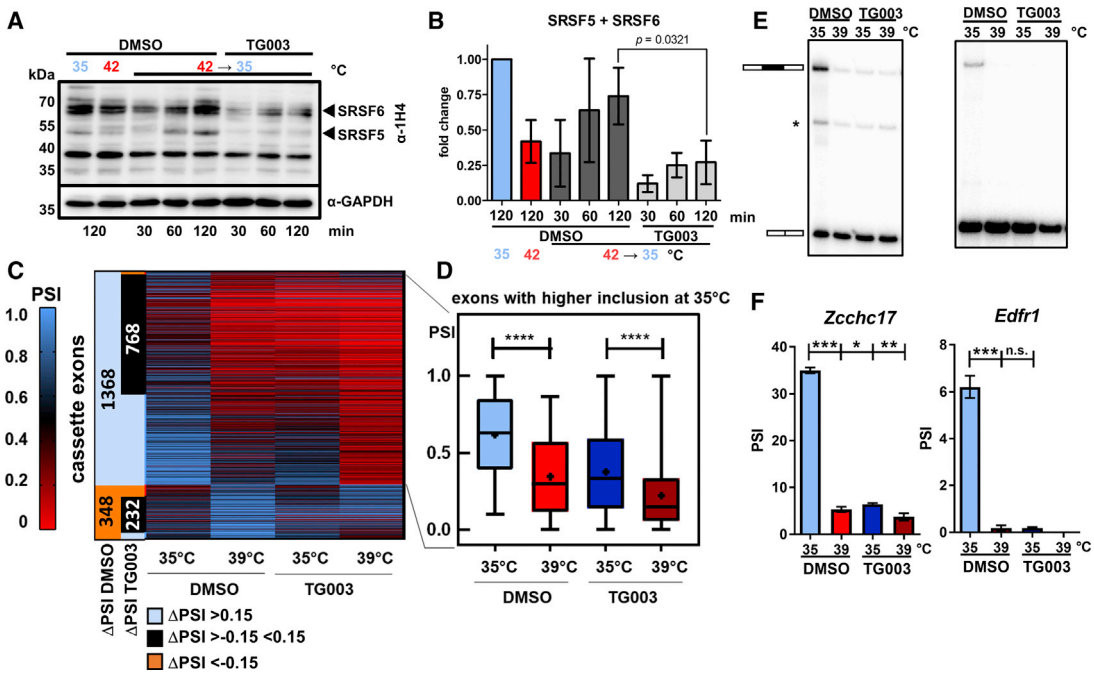

Figure 3. CLK Activity Controls Body-Temperature-Dependent SR Protein Phosphorylation and AS *In Vivo*

(A) HEK293 cells were incubated at 35°C overnight, then placed at 42°C for 120 min, treated with TG003 or DMSO, and shifted back to 35°C for 30, 60, or 120 min, respectively. A representative western blot with the Phospho-SR-specific antibody 1H4 is shown. GAPDH served as loading control.

(B) Quantification of western blots as in (A). Band intensities of two representative SR proteins at 70 kDa (SRSF6) and at 55 kDa (SRSF5) were quantified and normalized to the GAPDH loading control. Data represent mean of three independent sets ± SD. Statistical significance was determined by an unpaired t test.

(C and D) HEK293 cells were pre-entrained to 39°C for 12 h. After addition of DMSO or TG003, cells were shifted to 35°C (or maintained at 39°C); RNA was extracted after 6 h and analyzed by RNA-seq. In (C), a heatmap of percentage spliced in (PSI) values of all (1,745) skipped exon events that are temperature dependent in control (DMSO) is shown (n = 3). In the first two columns, events are classified based on their ΔPSI in DMSO and TG003 (35°C–39°C). In (D), box-whisker-plots (whiskers indicate min to max) of PSI values for exons with higher inclusion at 35°C are shown. The line represents the median PSI, and the cross represents mean PSI. Statistical significance is determined by 1-way ANOVA (Tukey's multiple comparisons test, ****$p < 1 \times 10^{-15}$). See also a comparison of ΔPSI values for DMSO and TG003 in Figure S2B.

(E and F) AS of *Zcchc17* and *Edfr1* was confirmed by radioactive RT-PCR. Representative gels are shown in (E) and quantified in (F) (n = 3, mean ± SD). Splicing isoforms, with or without the alternative exon (black box), are indicated on the left (E). Statistical significance was determined by unpaired t tests (F). For further targets, see Figures S2E and S2F.

See also Figure S2.

represents global and irreversible denaturation, as SRPK1 activity was not restored by shifting reactions back to 40°C (Figure 2B). This is in sharp contrast to the inactivation of CLKs at 38°C, which was quickly reversible when reducing the temperature from 38°C back to 34°C (Figures 2C and 2D). Additionally, we did not observe substantial changes in circular dichroism (CD) spectra of the human CLK1 KD at 25°C, 34°C, and 38°C, showing that the overall secondary structure remains intact at 38°C (Figure 2E). This observation is in line with a model in which increasing temperature first leads to subtle reversible changes in protein conformation (as in CLK1), followed by irreversible denaturation at higher temperature (as in SRPK1) (Thomas and Scopes, 1998). In summary, these *in vitro* data define CLK KDs as a molecular thermometer that is able to measure small changes in core body temperature to mediate downstream changes in (post-transcriptional) gene expression. In contrast to TRP channels that are involved in sensing changes in external temperature mainly outside of the body-temperature range (Wetsel, 2011), CLKs respond to endogenous temperature changes and are broadly expressed in diverse tissues, which could globally synchronize the body to changes in core temperature, e.g., in the circadian cycle.

CLK1/4 Act as Molecular Thermometer that Connects Physiological Temperature Changes with SR Protein Phosphorylation and AS in Human Cells

To confirm the role of CLK1/4 as molecular thermometer in living cells and to validate altered temperature-dependent SR protein phosphorylation as consequence, we used heat shock in human HEK293 cells as model system for an internal organ (kidney). A heat shock is known to induce hypophosphorylation of SR proteins (Shin et al., 2004), and shifting cells back to 35°C leads to rapid re-phosphorylation as assessed by the phospho-SR-specific 1H4 antibody (Figures 3A and 3B). We then performed heat shock recovery in the presence of the CLK1/4 inhibitor TG003 (Ninomiya et al., 2011) and indeed find that inhibition of CLK1/4 almost completely abolished re-phosphorylation of several SR proteins, including SRSF5 and SRSF6, when cells were shifted from 42°C to 35°C (Figures 3A and 3B). These data confirm that CLK1/4 are the main kinases controlling

temperature-dependent SR protein phosphorylation, as all temperature-dependent, 1H4 reactive bands (phosphorylated SR proteins) are also sensitive to TG003.

We then used RNA sequencing (RNA-seq) to investigate temperature-sensitive AS in HEK293 cell line as a downstream effect of altered SR protein phosphorylation. We obtained RNA-seq data from three independent samples from DMSO or TG003-treated cells incubated at 39°C or 35°C, respectively, corresponding to the temperatures of fever or mild hypothermia. While temperature-dependent AS has been investigated before, previous studies have used rather unphysiological conditions, e.g., 32°C or 42°C (Liu et al., 2013; Shalgi et al., 2014), and our data thus shed first light on global AS controlled by changes within the core body-temperature range. Using stringent filtering conditions, we identified around 1,700 cassette exons (see Table S1) with a temperature-dependent change in percentage spliced in (PSI) >15% in DMSO 35°C versus 39°C. Remarkably, adding the CLK1/4 inhibitor TG003 almost quantitatively blocked temperature-dependent AS, as the 35°C TG003 sample essentially matched the splicing pattern of the DMSO 39°C sample for the majority of variable exons (Figure 3C; see also Figure S2A for unsupervised clustering of replicate samples). Clustering these events by response in DMSO and TG003 shows that over 50% of cold- (768 of 1,368) and heat-induced (232 of 348) exons lose the temperature response upon TG003 treatment (delta PSI <15%, Figure 3C). To obtain another quantitative measure for this observation, we focused on cold-induced exons, which represent around 80% of the body-temperature-sensitive exons (Figure 3D). Interestingly, the mean PSI values for 39°C DMSO and 35°C TG003 are almost identical, indicating that at 35°C, TG003 quantitatively abolishes exon inclusion above the level observed at 39°C in DMSO treated samples. In addition, we find for many splicing events (and on average) that TG003 further increases the effect of warm temperature, probably through inhibiting residual CLK activity at 39°C. Finally, this analysis revealed a statistically significant reduced median PSI change in TG003-treated cells (Figure S2B), confirming a reduced temperature response in cells with inhibited CLK1/4. The remaining temperature response could indicate incomplete inhibition of CLKs or could indicate the presence of further thermometers acting in concert with CLK1/4 to control temperature-dependent AS. Similar results were obtained for intron retention events (Table S2; Figures S2C and S2D). Using splicing-sensitive RT-PCRs, the global trend was confirmed for 4 out of 4 tested targets (Figures 3E and 3F; Figures S2E and S2F). These data demonstrate that the majority of exons that are sensitive to changes in the body-temperature range also reacts to the inhibition of CLK1/4, which strongly argues that CLK1/4 are the dominant temperature sensors that connect body temperature with AS.

CLK1/4 Play a Major Role in Controlling Temperature-Sensitive Gene Expression

As discussed above, SR proteins control every aspect of (pre-) mRNA processing, from transcription to degradation. We therefore also analyzed temperature-dependent changes in whole transcripts in our RNA-seq dataset. We identified 1,064 genes whose abundance changed >1.3-fold between 35°C and 39°C in the DMSO control (Figure 4A; Table S3), which further underlines the global impact of physiological temperature changes on the cellular gene expression program. Notably, around 50% of these genes (507) lose temperature sensitivity in TG003-treated cells (genes with <1.3-fold between 35°C and 39°C in TG003-treated cells are boxed in Figure 4A; see also Figure 4B for examples with abolished temperature-dependent gene expression; Table S3). These data confirm that CLK1/4 are the dominant thermo-sensors that sense changes in the physiologically relevant temperature range to then control AS and gene expression.

One of the mRNAs that is strongly temperature-responsive only in control cells encodes for the CIRBP (Figure 4B). Cold-induced expression of CIRBP has been suggested to provide a link between the circadian clock, sleep, and body temperature (Hoekstra et al., 2019; Morf et al., 2012). CIRBP also plays an important role in hypothermia, cancer, and inflammation (Lujan et al., 2018; Qiang et al., 2013) and has been implicated in TSD in turtles (Schroeder et al., 2016). Despite the central importance of cold-induced CIRBP expression, it remains unclear how a reduction in temperature increases CIRBP expression mechanistically. Given our finding that cold-induced CIRBP expression is completely abrogated in TG003-treated cells (Figure 4B), we chose CIRBP for a more detailed analysis. Interestingly, our splicing analysis revealed an alternative 3′ end in the *Cirbp* mRNA, which is strongly promoted by higher temperature in the DMSO control but almost temperature insensitive in TG003-treated cells (Figure 4C). In this warm-induced isoform, instead of the canonical last exon 7a, an alternative exon 7b is used, which is coupled to exon 8 inclusion (Figure 4C, red). We observe strong evolutionary conservation downstream of the canonical polyadenylation site including the 3′ splice site of exon 7b in all vertebrates (Figure 4C, bottom; Figure S2G), including turtles and alligators (see below). Consistent with an evolutionarily conserved mechanism and function, we also observed warm-induced generation of the exon 7b isoform in primary mouse hepatocytes (Figure S2H). Additionally, we found that young mice exposed to a lower ambient temperature, resulting in decreased body temperature (Preußner et al., 2017), show reduced exon 7b inclusion in liver, which correlates with increased total *Cirbp* expression (Figure 4D), which we also observed in primary hepatocytes from adult mice (Figure S2I), thus confirming regulation *in vivo*. To mechanistically link this splicing event with the temperature-regulated differences in gene expression, we made use of CRISPR/Cas9 and generated cell lines lacking exons 7b to 8 in human HEK293 cells (Figure 4E). These cells show increased *Cirbp* mRNA levels and a decreased response to temperature (Figure 4F). Some residual temperature dependence could be mediated via altered general splicing efficiency (Gotic et al., 2016) or warm-induced retention of intron 6, which interestingly is also directly responsive to changes in body temperature (Horii et al., 2019). Together, these data are consistent with a model, in which warm-induced inclusion of exon 7b results in an mRNA with reduced stability and therefore reduced total gene expression. An analogous mechanism could be globally responsible for the observed temperature and TG003-dependent differences in gene expression, which would actually reflect splicing changes that control mRNA stability,

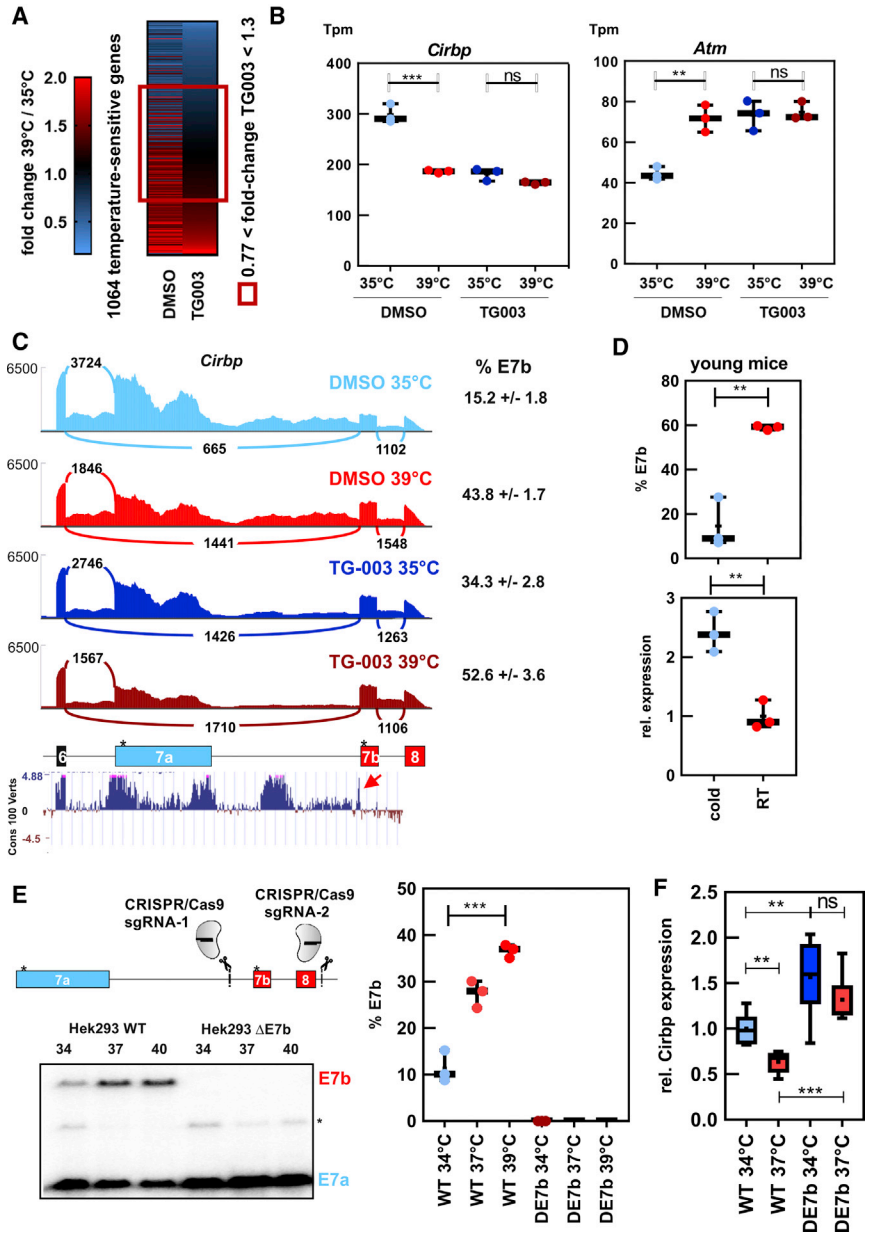

Figure 4. CLK Activity Controls Body-Temperature-Dependent Gene Expression

(A) Heatmap of 1,064 genes with >1.3-fold changed gene expression in DMSO. Plotted is the expression at 39°C relative to the expression at 35°C. Genes are sorted by the fold change in TG003; the red box highlights genes with a fold change <1.3 in TG003 (n = 507).

(B) Examples with abolished temperature-dependent gene expression. Plotted are the transcripts per million (tpm) values from the three biological replicates. Whiskers indicate min to max. Statistical significance was determined by an unpaired t test. Note that temperature-dependent gene expression is basically abolished upon TG003 treatment.

(C) Temperature-dependent AS of the *Cirbp* 3′ end. Sashimi blots show the read distribution for the different conditions (y axis set to 6,500 reads per base). The curved lines indicate RNA-seq reads which span the junction of two exons (the numbers represent independent reads confirming this junction). Percentage of the E7b isoform was calculated in the triplicate samples, and mean and standard deviation are depicted on the right. Below, exon/intron structure of the pre-mRNA is shown. Exons are depicted by boxes, introns are depicted by lines, and the asterisks indicate stop codons. At the bottom, basewise comparison across 100 vertebrates by PhyloP from the UCSC genome browser is shown. The red arrowhead marks the conserved 3′ splice site of exon 7b. See also Figure S2G.

(D) *Cirbp* splicing and gene expression in the liver of young mice (12–13 days) kept at room temperature (RT) or at 18°C for 2 h (cold, see Preußner et al., 2014 for post-mortem temperatures). Splicing was analyzed by splicing-sensitive RT-PCR with a forward primer in exon 6 and two reverse primers in exons 7a and 7b, and gene expression was analyzed by RT-qPCR and is shown normalized to *Hprt* and RT (n = 3, plotted are values from individual biological replicates; whiskers indicate min to max). Statistical significance was determined by unpaired t tests, **p < 0.01.

(E) Depletion of exons 7b-8 using CRISPR/Cas9 in HEK293 cells (top: position of guide RNAs), below a radioactive RT-PCR investigating *Cirbp* AS at the indicated temperatures is shown and quantified (right, n = 3, plotted are single replicate values; whiskers indicate min to max). Statistical significance was determined by unpaired t tests, ***p < 0.001.

(F) Increased and less temperature-dependent *Cirbp* expression in cells lacking the temperature-dependent exon 7b. *Cirbp* expression was investigated after 12 h at the indicated temperatures by RT-qPCR and is plotted in a box-whisker blot with lines representing median and cross representing mean expression levels (relative to *Gapdh*, n > 5, statistical significance was determined by unpaired t tests, **p < 0.01, ***p < 0.001).

See also Figure S2.

e.g., through inducing nonsense-mediated decay (NMD), to eventually control gene expression. Indeed, we find that 149 of 1,064 the temperature-dependent genes also contain at least one temperature-dependent cassette exon (Figure S2J), and skipping of these exons leads, in the majority of cases (63%), to a frameshift, probably triggering NMD. However, in addition to NMD other mechanisms downstream of SR protein phosphorylation probably contribute to the regulation of temperature-dependent gene expression.

Mechanistic and Structural Basis for Temperature-Controlled CLK1/4 Activity

The general structure of the CLK and SRPK KDs is similar (Bullock et al., 2009), providing a well-suited system to identify mechanistic and structural details of the CLK-specific thermosensor (see Figures S3A–S3D for a comparison of SRPK, CLK, and the model kinase PKA and superposition of the PKA substrate with the CLK active center). Based on published structures of human CLK1 and SRPK, we initially performed molecular

Mutanti fatti come??????

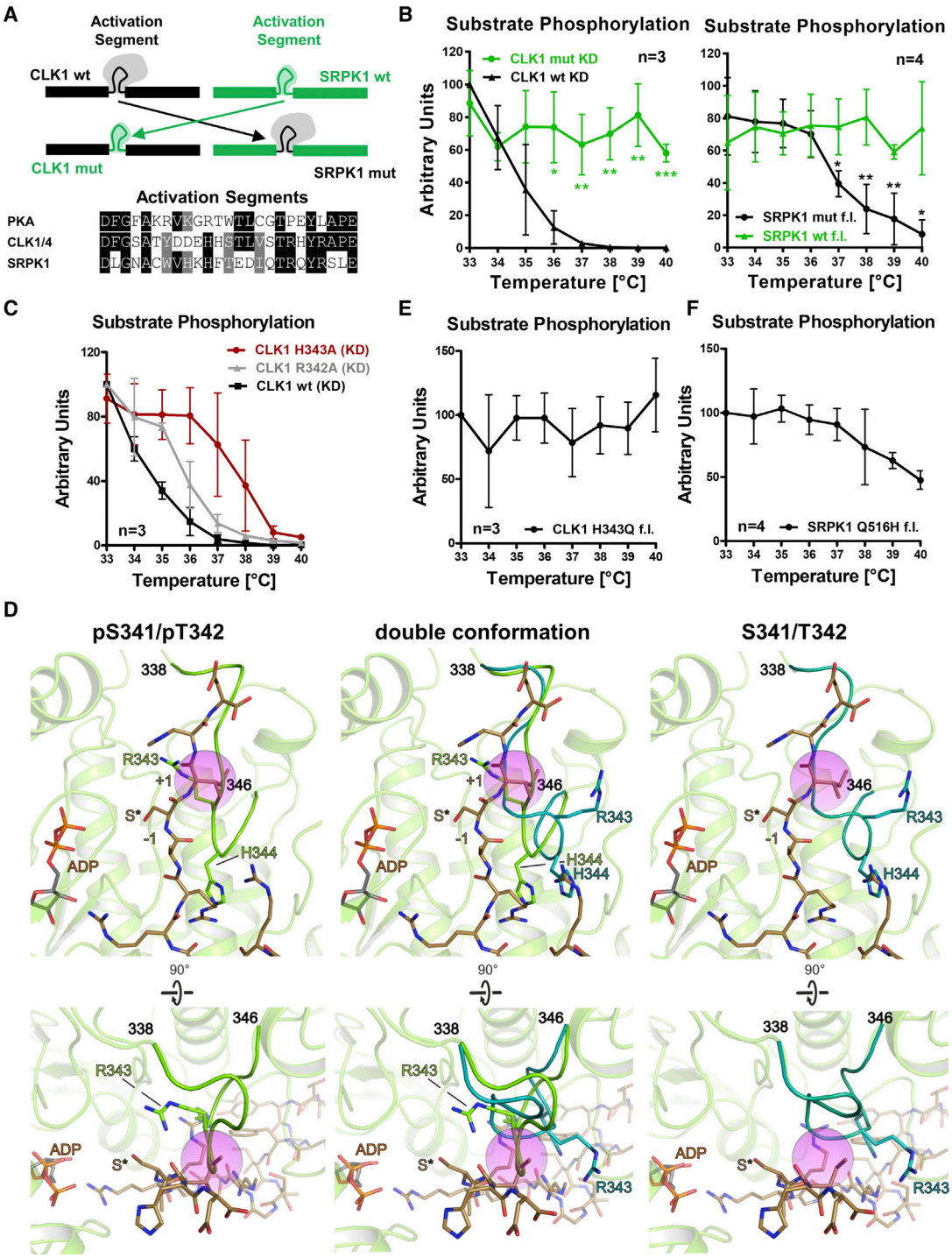

Figure 5. Temperature Sensitivity of CLK Activity Is Mediated through a Conserved His Residue in the Activation Segment

(A and B) Generation of activation segment switch hybrids (A) leads to loss and gain of temperature sensitivity (B; n = 3, mean ± SD, statistical significance was investigated by an unpaired t test *p < 0.05, **p < 0.01, ***p < 0.001). Activation segment mutants are based on MD simulations (Figure S3E). Temperature-dependent activity was determined as in Figure 1B. See also Figures S3G–S3J for gel images and quantification of autophosphorylation. At the bottom of (A), an alignment of the activation segments of CLK1/4 and SRPK1 is shown in comparison to the model kinase PKA.

(C) Quantification of CLK1 kinase domain WT, R342A, and H343A activities (mean ± SD). R342A and H343A represent the variants with the strongest effect on the temperature-activity profile; see Figures S4A and S4B for the full alanine scan.

(legend continued on next page)

dynamics (MD) simulations at 20°C and 40°C, the temperatures that experimentally show maximal and completely lost CLK1 activity, respectively (Figure 2A). During MD simulations, the overall structure of the KD remained unchanged at the two temperatures (Figure S3E), which is in agreement with our CD spectroscopy data and consistent with subtle and reversible structural changes mediating temperature sensitivity. However, the CLK, but not the SRPK, activation segment shows higher flexibility and an altered conformation at 40°C (Figures S3E and S3F; Videos S1 and S2). The activation segment is an essential and kinase-specific (Eswaran et al., 2008; Taylor and Radzio-Andzelm, 1994) ~25 residue region (Bullock et al., 2009; Nolen et al., 2004) whose conformation in the active center of the kinase determines kinase activity. As no other region within the CLK1 KD showed substantial temperature-dependent differences (Figures S3E and S3F), we hypothesized that the CLK activation segment could act as thermo-sensor. To test this idea, we created chimeric kinases with exchanged activation segments (Figure 5A). Indeed, CLK1 containing the SRPK1 activation segment lost all temperature sensitivity and SRPK1 containing the CLK1/4 activation segment became temperature sensitive in a range similar to CLK1 itself (Figures 5B and S3G–S3J). Therefore, the CLK activation segment is necessary and sufficient to mediate sensitivity to changes in the physiological temperature range. Additionally, the activation segment is 100% conserved between mouse and human CLK1 and CLK4, suggesting a conserved and essential function.

To further address the molecular basis for temperature sensitivity, we performed an alanine scan of the activation segment in the context of the KD (Figure S4A). While most active mutants displayed a temperature-activity profile as the wild-type (WT) kinase, mutations of two neighboring amino acid residues, R342 and H343, showed a shift toward a higher inactivation temperature (Figures 5C and S4B). This was especially pronounced for the H343A mutant, which remained fully active at 36°C, a temperature where the activity of the WT enzyme is already below 20% (Figures 5C, S4A, and S4B). In our MD simulations, these two residues are found in close proximity to the ATP in the active center of the kinase only at 40°C (Videos S1 and S2), whereas especially H343 is far away from the active center at 20°C (Figure S4C). R342 and H343 are part of the P+1 loop, a part of the activation segment that makes contact to the substrate, and in fact the conformation of the whole P+1 loop changes in a temperature-dependent manner (Figures S4E–S4G). To provide further evidence for conformational heterogeneity of the CLK activation segment, we compared available crystal structures. The published CLK structure obtained in a complex with an inhibitor (PDB: 2VAG [Fedorov et al., 2011]) represents an interesting example, as double phosphorylation of S341 and T342 induces an altered conformation of the activation segment. Here, both phosphorylated residues are rotated from an inside faced to an outward faced orientation, that in consequence alters the conformation of R343 and H344 (Figures 5D and S4D). Interestingly, when reevaluating the electron density, we observed a double conformation of the activation segment (Figures 5D and S4D; Table S4; PDB: 6TW2). The second, so far not modeled, conformation does not contain the two phosphorylated residues and matches the previously described active CLK conformation (PDB: 1Z57; Figure S4D). We overlaid the three crystal structures with our simulated structures obtained at 20°C and 40°C and again observed different conformations of the P+1 loop, especially when comparing our 40°C model with the canonical, active structure (PDB: 1Z57) (Figures S4H–S4K). Differences may also be partly due to the low temperature (4°C) at which the crystals were grown (Bullock et al., 2009; Fedorov et al., 2011) or the freezing of crystals prior to the measurement. Interestingly, two conformations, our 40°C MD structure and the phosphorylated CLK1 (PDB: 2VAG and 6TW2) structure both show the histidine and arginine residues oriented toward the substrate binding grove (Figure S4K). To address potential consequences of an altered P+1 loop conformation we superimposed the available CLK1 crystal structures with a model (PKA) substrate (Figures S3A–S3D), as no structure of an SR substrate bound to the active center of the CLK is available. This clearly showed that in the diphosphorylated CLK1 structure (PDB: 2VAG and 6TW2; Figures 5D and S5A) and at 40°C (Figures S4G, S4I, and S4K) the P+1 loop adopts a conformation that is likely to interfere with substrate binding, especially around the target serine.

Our MD data suggest that a conformational change in H343 pushes R342 toward the substrate binding groove, which is consistent with the increased distance between R343 and ATP that we observe in MD simulations of the H344A mutant at 40°C (Figure S4C, bottom). The histidine residue is conserved in all temperature-sensitive CLKs tested (see below for more temperature-dependent CLK homologs from different species all containing R and H residues at the respective positions), whereas it is replaced by a glutamine in the temperature-insensitive SRPK1 (Figure 5A). Remarkably, a H343Q mutation in f.l. CLK1 is sufficient to abolish temperature sensitivity altogether, and the corresponding point mutant in SRPK (Q516H) renders the enzyme temperature sensitive (Figures 5E, 5F, and S5B–S5D), thus validating our MD simulations and confirming a crucial role of a single amino acid residue in mediating temperature sensitivity.

To address whether this holds true in living cells, we overexpressed either the WT CLK1 or the H343Q mutant in HEK293 cells and indeed observed that warm-induced exon skipping is

(D) Re-refined structure of the activation segment of CLK1 (PDB: 6TW2) with a superimposed PKA substrate peptide (PDB: 1JBP). On the left, the previously described conformation (Fedorov et al., 2011) with double-phosphorylated pS341/pT342 is shown in chartreuse. On the right, the conformation with unphosphorylated S341/T342 is shown in teal. In the middle, the double conformation is shown. The substrate is shown in stick presentation and colored in light brown. The sphere indicates a region for a potential sterical clash of substrate and kinase, especially in the phosphorylated conformation. Residues in human CLK1 are shifted by +1 in comparison to the respective mouse residues. The re-refined overall structure is shown in Figure S5A in an identical orientation.
(E) H343 is required for temperature sensitivity. A kinase assay with the CLK1 H343Q mutant is shown as in (B) (n = 3, mean ± SD; also see Figures S5B and S5C for gel images and autophosphorylation).
(F) A single G-to-Q mutation renders SRPK1 temperature sensitive. A kinase assay with the SRPK1 f.l. Q516H mutant is shown as in (B) (n = 3, mean ± SD); also see Figure S5D for gel images.
See also Figures S3–S5.

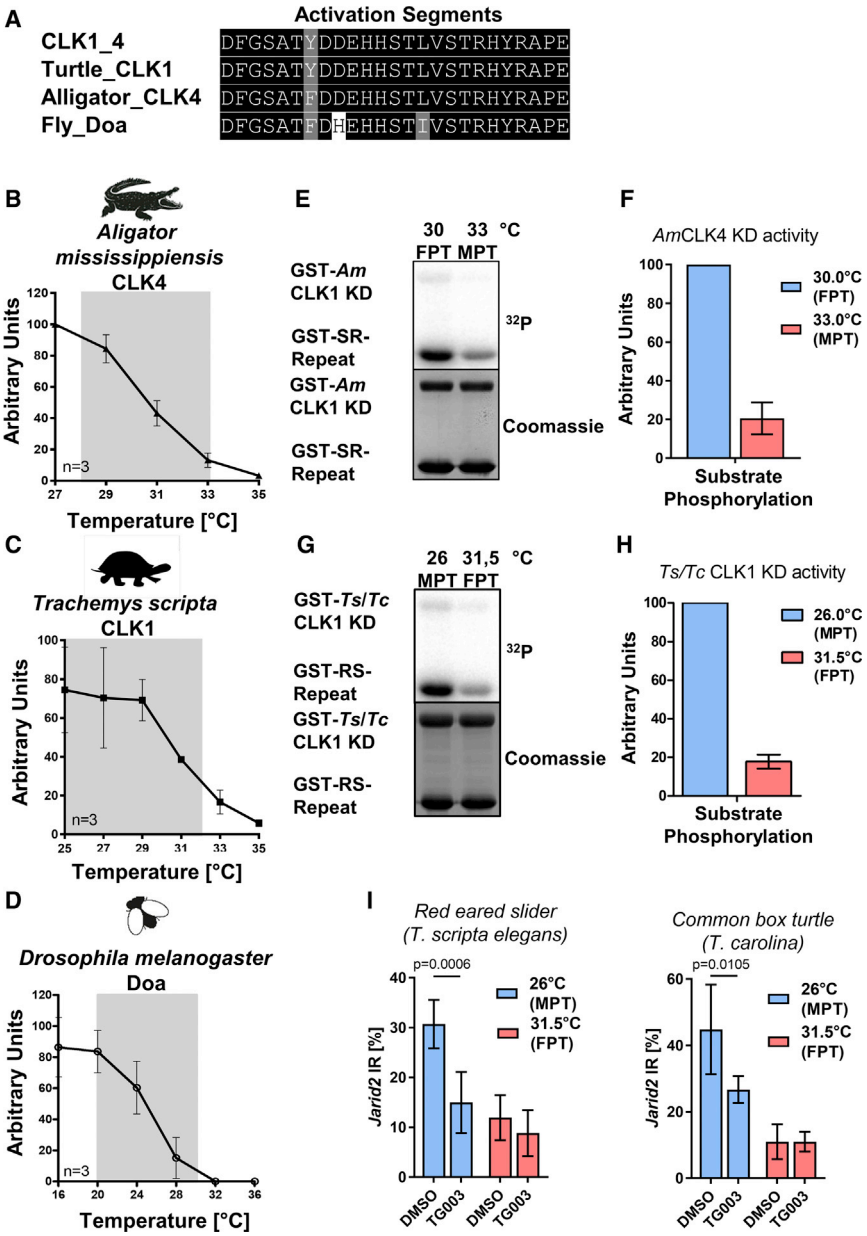

Figure 6. Temperature-Dependent Activity of Poikilothermic CLK Homologs Is Evolutionarily Adapted

(A) Alignment of activation segments from human (identical in mouse) CLK1/4 and homologous kinases from alligator (CLK4), turtle (CLK1), and fly (DOA).

(B–D) Temperature sensitivity of alligator (B), turtle (C), and fly (D) CLK homologs falls into the range of preferred living temperatures (gray boxes). Kinase activity is plotted as mean ± SD (n = 3). For gel images, see Figures S6A–S6C.

(E and F) The activity of the alligator CLK4 was investigated at female-producing temperature (FPT, 30°C) or male-producing temperature (MPT, 33°C). A representative gel is shown in (E); quantifications of substrate phosphorylation are shown in (F) (n = 3, mean ± SD).

(G and H) The activity of the turtle CLK1 kinase domain (identical in *Trachemys scripta* and *Terrapene carolina*) was investigated at MPT (26°C) FPT (31.5°C [Czerwinski et al., 2016]). A representative gel is shown in (G), and quantifications of substrate phosphorylation are in (H) (n = 3, mean ± SD).

(I) Quantification of an intron retention event involved in TSD in two independent turtle cell lines (*T. carolina* and *T. scripta*, cell lines established from heart and spleen tissue, respectively) at MPT or FPT with or without the CLK inhibitor TG003, using RT-qPCR. Data represent mean ± SD of three independent experiments. Statistical significance was determined by unpaired t tests.

See also Figure S6.

altered by overexpression of the temperature-insensitive H343Q mutant (Figures S5E–S5G), confirming that the *in vitro* mutagenesis data are applicable to living cells. These results thus suggest a mechanistic basis for body-temperature-controlled kinase activity. In addition, the finding that a single residue exchange can completely abolish temperature sensitivity (H343Q) or shift the temperature optima (R342A, H343A) opens the possibility to engineer designer kinases with a defined temperature-activity profile.

CLK1/4 Activity Is Evolutionarily Adapted to the Growth Temperature of Poikilotherms

Poikilotherms, in contrast to homeotherms, adapt to the ambient temperature and thus experience stronger variations in body temperature. To address whether the CLK-based temperature-sensing mechanism is evolutionarily conserved and adapted to the respective growth temperatures, we tested the temperature-activity profiles of CLK homologs from three poikilothermic species. We chose two reptilian species, alligator and turtle, and the fly, *D. melanogaster*, as a model organism that has separated from reptiles ~1 billion years ago (see Figure 6A for a comparison of the activation segments). For all three organisms, we find that the activity of the CLK homologs are switched off at the upper limit of the physiologically relevant temperature ranges (Figures 6B–6D and S6A–S6C), which matches our observation for mammalian CLKs. Of note, the reptilian CLK temperature-activity profiles are markedly different from the mouse version in this temperature range, confirming species specificity (Figure S6D). These temperature-activity profiles with higher activity in the lower range of the physiologically relevant temperature of diverse organisms show that the mechanism and regulatory principle is conserved across evolution but that the enzymes have adapted to the respective physiological temperature range. This furthermore indicates a conserved and evolutionarily adapted function of CLKs in adapting gene expression to the changes in body temperature experienced by the respective organisms.

Interestingly, in diverse reptiles sex determination is controlled by the temperature at which eggs are incubated (Capel, 2017); for example, for the American alligator incubating eggs below 30°C will result in females, whereas temperatures between 30°C and 34°C will yield mostly male offspring (Ferguson and Joanen, 1982). While this has been known for decades, the thermo-sensor that initiates sex determination has remained elusive (Georges and Holleley, 2018). Notably, the temperature-activity profile of the alligator CLK4 falls exactly within the range of temperature-dependent sex determination (Figures 6B, 6E, and 6F; see also Figure S6E for f.l. CLK4). Similarly, for the turtle CLK1, we observe full activity below 26°C and a strong reduction, around 10% remaining activity, above 31°C, basically representing an on-off switch in the temperature range of sex determination (Figures 6C, 6G, and 6H; see also Figure S6F for f.l. CLK1). The regulated activity of CLK kinases from two independent reptilian species, exactly in the temperature range for sex determination, suggests that CLK enzymes may represent a temperature sensor for TSD in reptiles. Recent studies have associated temperature-dependent AS, in this case intron retention events in Jumonji histone deacetylases, with TSD (Deveson et al., 2017; Ge et al., 2018). To investigate whether these AS events are CLK dependent, we used cell lines from two different turtle species (red eared slider turtle and common box turtle). We first confirmed temperature-dependent intron retention of intron 18 in *Jarid2*, a Jumonji-domain-containing chromatin modifier, which is involved in TSD (Deveson et al., 2017). As in the *in vivo* situation, we find substantially increased intron retention at the male-producing, lower temperature (26°C) than at the female-producing 31.5°C in both cell lines (Figure 6I). We then repeated the experiment in the presence of the CLK1/4 inhibitor TG003 (which was active in inhibiting the turtle kinase *in vitro*, Figures S6G and S6H). TG003 had little effect on *Jarid2* intron retention at 31.5°C, where the turtle CLK1 is not active (Figure 6I). However, TG003 prevented the increased intron retention in *Jarid2* at colder temperature, providing evidence that a TSD-associated AS event is controlled by temperature-dependent CLK activity. Our combined data show that body-temperature-mediated control of CLK activity is conserved across evolution and adapted to the respective temperature range of diverse organisms and implicate cold-induced CLK activity in TSD in reptiles.

DISCUSSION

Here, we describe the activity of CLKs to be controlled by subtle changes in (body) temperature. This extreme temperature sensitivity is an inherent feature of the kinases, as it is observed in recombinant proteins purified from bacteria. It does not require allosteric modulators, posttranslational modifications, or interaction partners, thus representing a paradigm-setting example for the regulation of enzymatic activity in the physiologically relevant temperature range. Various studies have shown that phosphorylation within the activation segment is crucial for the activity of many kinases, as it induces an ordered conformation essential for activity (Goldberg et al., 1996; Huse and Kuriyan, 2002; Johnson et al., 1996). However, in the CLK1/3 crystal structure the activation segment is not phosphorylated but has an ordered, active conformation (Bullock et al., 2009), suggesting that, for CLKs, and potentially other kinases or enzymes in general, temperature-controlled conformational changes may play a similar role. This kinase-based thermo-sensor represents a cellular thermometer that, in contrast to TRP channels, which are mainly reacting to external temperature, reacts to endogenous core body-temperature changes. The precise mechanism that renders the conformation of the activation segment, in particular, the P+1 loop, temperature sensitive, as well the molecular details that control kinase activity remains to be determined. The P+1 loop is engaged in kinase-substrate interaction (Nolen et al., 2004), and repositioning of this loop may thus alter substrate binding. Indeed, our MD simulations and analysis of existing crystal structures, in particular, a structure containing a double-phosphorylated P+1 loop (Fedorov et al., 2011), show structural flexibility of this part of the activation segment and point to the existence of structures that interfere with substrate binding. However, other mechanisms could equally well alter kinase activity in a temperature-dependent manner. One interesting possibility would be reduced processivity at higher temperature. As we find both auto- and substrate phosphorylation to be temperature dependent, and autophosphorylation is most likely not dependent on kinase processivity, this mechanism seems unlikely to entirely explain temperature sensitivity. Room temperature X-ray crystallography (Henzler-Wildman and Kern, 2007; Weik and Colletier, 2010), temperature resolved structure determination (Thompson et al., 2019), or temperature resolved nuclear magnetic resonance (NMR) are methods that will eventually yield insights into molecular interactions that govern temperature-dependent conformational changes and the connection to altered kinase activity. The direct consequence is altered SR protein phosphorylation, which is involved in all (pre-)mRNA processing events, from transcription to splicing, nuclear export, translation, and stability (Long and Caceres, 2009; Maslon et al., 2014; Müller-McNicoll et al., 2016; Zhong et al., 2009). The example of CIRBP highlights how a temperature-controlled AS event can also generate temperature-dependent differences in gene expression. Many more temperature and TG003-dependent mRNAs could be controlled by a similar splicing-based mechanism. This could be achieved through temperature-dependent splicing isoforms with reduced stability, e.g., due to a shorter 3′ UTR or containing premature stop codons inducing NMD.

This cellular thermometer has far-reaching functional implications in diverse physiological and pathophysiological conditions. For example, our work directly connects circadian changes in body temperature with posttranscriptional control of gene expression, which will have a substantial impact on diverse aspects of physiology. As core body temperature decreases with aging (Keil et al., 2015), we also provide a possible mechanism that controls AS and gene expression in general in the aging population. Given the sensitivity and the quick reaction to small temperature changes, CLK activity is likely to also impact on gene expression in pathological conditions such as hypothermia, septic shock, and fever, or in the slightly warmer tumor microenvironment. Similarly, processing of viral transcripts, such as HIV or influenza pre-mRNA has been shown to be dependent on CLKs and host SR proteins (Artarini et al., 2019; Wong et al., 2013) and may thus be controlled through body temperature.

In addition, our data from poikilotherms indicate an evolutionarily conserved and adapted function in temperature sensing with fundamental importance, as our analysis suggests an involvement in reptilian sex determination. It is interesting to note that lower temperature induces an intron retention isoform of Jumonji-domain-encoding mRNAs (*Jarid2* and *Kdm6b*) in turtle and alligator, whereas intron retention isoforms are induced by warmer temperatures in the bearded dragon *Pogona vitticeps* (Deveson et al., 2017). We suggest that cold-induced CLK activity controls SR protein phosphorylation, which then regulates intron retention. As the binding position of SR proteins relative to the regulated intron/exon determines the effect on splicing (Erkelenz et al., 2013), exclusion or inclusion, we suggest that this accounts for the opposite effects of temperature on intron retention in different species. Formation of the intron retention isoforms is associated with sex determination, but the functionality of the resulting proteins and a potential role in initiating or stabilizing sex determination remains to be shown. Of note, we find an intron retention event in human *Kdm6b* to be temperature and TG003 sensitive (Table S2), suggesting wide evolutionary conservation.

As it is plausible to assume that a fundamental decision such as sex determination requires input from more than one signaling pathway, e.g., separate signals for initiation and stabilization, we suggest that CLKs are one, but not necessarily the only, molecular thermometer contributing to TSD. Interestingly, temperature-dependent *Cirbp* expression has also been linked to TSD in turtles (Schroeder et al., 2016). As we show that cold-induced *Cirbp* expression is also dependent on AS and CLK activity, our data provide evidence that CLKs control at least two independent events, intron retention in chromatin modifiers and *Cirbp* expression, that are implicated in TSD. As CIRBP has been hypothesized to control expression of *Kdm6b* (Georges and Holleley, 2018), these pathways may eventually interact, to increase expression of the intron-retained Kdm6b isoform at colder temperature (in turtles), which has been suggested to be a crucial event in TSD (Ge et al., 2018).

Finally, our mechanistic analysis reveals individual amino acid residues that are crucial to set the temperature range in which CLKs are inactivated. This opens the possibility to engineer kinases with defined temperature-activity profiles. Such kinases may be used as reversible on-off switches in cell culture and in gene therapeutic applications and potentially to alter temperature sensing of whole organisms, which may become especially relevant in light of global warming.

STAR★METHODS

Detailed methods are provided in the online version of this paper and include the following:

- KEY RESOURCES TABLE
- LEAD CONTACT AND MATERIALS AVAILABILITY
- EXPERIMENTAL MODEL AND SUBJECT DETAILS
  - Mouse maintenance
  - Tissue culture cells
- METHOD DETAILS
  - Cloning and Protein purifications
  - Kinase assay
  - Cell culture, RNA extraction, RT-PCRs, Transfection and western blot
  - Investigation of AS and gene expression by RNA sequencing
  - Generation of CRISPR-Cas9 edited cells and analysis of Cirbp expression
  - Molecular Dynamics Simulation
  - CD-spectroscopy
  - Crystallographic procedures
- QUANTIFICATION AND STATISTICAL ANALYSIS
- DATA AND CODE AVAILABILITY

SUPPLEMENTAL INFORMATION

Supplemental Information can be found online at https://doi.org/10.1016/j.molcel.2020.01.028.

ACKNOWLEDGMENTS

The authors would like to thank Jan Driller (FU Berlin) for providing SRPK1 protein, Ana Rita Lima Fernandes and Dorian Mikolajczak from the AG Koksch (FU Berlin) for help with CD spectroscopy, Sutapa Chakrabarti (FU Berlin) for discussion, and members of the Heyd lab for comments on the manuscript. We thank Matthias Lenk from the Friedrich-Loeffler-Institut (Greifswald, Germany) for providing turtle cell lines. The expression construct for human SRPK1 was kindly provided by Gourisankar Ghosh (UCSD). Computational resources provided by the North-German Supercomputing Alliance (HLRN) are gratefully acknowledged. P.I. thanks Philip Ulrich for help with vmd/tcl scripting. F.H. thanks Jan Medenbach (Regensburg University) for discussing sex determination in reptiles. This work was funded through DFG grants HE5398/4 and HE5398/4-2 to F.H.; additional funding was provided by the DFG grant 278001972 - TRR 186 to F.H. and M.C.W. M.P. is funded by a post doc stipend of the Peter and Traudl Engelhorn Foundation.

AUTHOR CONTRIBUTIONS

T.H., A.K., and M.P. performed most experiments with help from F.D.B., A.F., and S.S.; protein purifications were done in M.C.W.'s lab, and B.L. performed most structural analysis. A.-K.E., K.K.P., and S.M. generated and characterized *Cirbp*-edited cell lines. M.P. performed bioinformatics analysis. B.T. performed RNA sequencing. P.I. performed MD simulations. T.H., M.P., and F.H. designed the study, planned experiments, analyzed data, and wrote the manuscript, with input from P.I., B.L., and M.C.W. F.H. conceived and supervised the work.

DECLARATION OF INTERESTS

The authors declare no competing interests.

Received: October 30, 2019
Revised: December 12, 2019
Accepted: January 27, 2020
Published: February 13, 2020

REFERENCES

Adams, P.D., Afonine, P.V., Bunkóczi, G., Chen, V.B., Davis, I.W., Echols, N., Headd, J.J., Hung, L.W., Kapral, G.J., Grosse-Kunstleve, R.W., et al. (2010). PHENIX: a comprehensive Python-based system for macromolecular structure solution. Acta Crystallogr. D Biol. Crystallogr. *66*, 213–221.

Afonine, P.V., Grosse-Kunstleve, R.W., Echols, N., Headd, J.J., Moriarty, N.W., Mustyakimov, M., Terwilliger, T.C., Urzhumtsev, A., Zwart, P.H., and Adams, P.D. (2012). Towards automated crystallographic structure refinement with phenix.refine. Acta Crystallogr. D Biol. Crystallogr. *68*, 352–367.

Artarini, A., Meyer, M., Shin, Y.J., Huber, K., Hilz, N., Bracher, F., Eros, D., Orfi, L., Keri, G., Goedert, S., et al. (2019). Regulation of influenza A virus mRNA splicing by CLK1. Antiviral Res. *168*, 187–196.

Aubol, B.E., Wu, G., Keshwani, M.M., Movassat, M., Fattet, L., Hertel, K.J., Fu, X.D., and Adams, J.A. (2016). Release of SR Proteins from CLK1 by SRPK1: A Symbiotic Kinase System for Phosphorylation Control of Pre-mRNA Splicing. Mol. Cell *63*, 218–228.

Bautista, D.M., Siemens, J., Glazer, J.M., Tsuruda, P.R., Basbaum, A.I., Stucky, C.L., Jordt, S.E., and Julius, D. (2007). The menthol receptor TRPM8 is the principal detector of environmental cold. Nature *448*, 204–208.

Best, R.B., Zhu, X., Shim, J., Lopes, P.E.M., Mittal, J., Feig, M., and Mackerell, A.D., Jr. (2012). Optimization of the additive CHARMM all-atom protein force field targeting improved sampling of the backbone φ, ψ and side-chain χ(1) and χ(2) dihedral angles. J. Chem. Theory Comput. *8*, 3257–3273.

Buhr, E.D., Yoo, S.H., and Takahashi, J.S. (2010). Temperature as a universal resetting cue for mammalian circadian oscillators. Science *330*, 379–385.

Bullock, A.N., Das, S., Debreczeni, J.E., Rellos, P., Fedorov, O., Niesen, F.H., Guo, K., Papagrigoriou, E., Amos, A.L., Cho, S., et al. (2009). Kinase domain insertions define distinct roles of CLK kinases in SR protein phosphorylation. Structure *17*, 352–362.

Bussi, G., Donadio, D., and Parrinello, M. (2007). Canonical sampling through velocity rescaling. J. Chem. Phys. *126*, 014101.

Capel, B. (2017). Vertebrate sex determination: evolutionary plasticity of a fundamental switch. Nat. Rev. Genet. *18*, 675–689.

Charkoudian, N., Hart, E.C.J., Barnes, J.N., and Joyner, M.J. (2017). Autonomic control of body temperature and blood pressure: influences of female sex hormones. Clin. Auton. Res. *27*, 149–155.

Chen, V.B., Arendall, W.B., 3rd, Headd, J.J., Keedy, D.A., Immormino, R.M., Kapral, G.J., Murray, L.W., Richardson, J.S., and Richardson, D.C. (2010). MolProbity: all-atom structure validation for macromolecular crystallography. Acta Crystallogr. D Biol. Crystallogr. *66*, 12–21.

Colwill, K., Pawson, T., Andrews, B., Prasad, J., Manley, J.L., Bell, J.C., and Duncan, P.I. (1996). The Clk/Sty protein kinase phosphorylates SR splicing factors and regulates their intranuclear distribution. EMBO J. *15*, 265–275.

Czerwinski, M., Natarajan, A., Barske, L., Looger, L.L., and Capel, B. (2016). A timecourse analysis of systemic and gonadal effects of temperature on sexual development of the red-eared slider turtle Trachemys scripta elegans. Dev. Biol. *420*, 166–177.

Deveson, I.W., Holleley, C.E., Blackburn, J., Marshall Graves, J.A., Mattick, J.S., Waters, P.D., and Georges, A. (2017). Differential intron retention in *Jumonji* chromatin modifier genes is implicated in reptile temperature-dependent sex determination. Sci. Adv. *3*, e1700731.

Dominguez, D., Tsai, Y.H., Weatheritt, R., Wang, Y., Blencowe, B.J., and Wang, Z. (2016). An extensive program of periodic alternative splicing linked to cell cycle progression. eLife *5*. Published online March 25, 2016. https://doi.org/10.7554/eLife.10288.

Emsley, P., Lohkamp, B., Scott, W.G., and Cowtan, K. (2010). Features and development of Coot. Acta Crystallogr. D Biol. Crystallogr. *66*, 486–501.

Erkelenz, S., Mueller, W.F., Evans, M.S., Busch, A., Schöneweis, K., Hertel, K.J., and Schaal, H. (2013). Position-dependent splicing activation and repression by SR and hnRNP proteins rely on common mechanisms. RNA *19*, 96–102.

Eswaran, J., Bernad, A., Ligos, J.M., Guinea, B., Debreczeni, J.E., Sobott, F., Parker, S.A., Najmanovich, R., Turk, B.E., and Knapp, S. (2008). Structure of the human protein kinase MPSK1 reveals an atypical activation loop architecture. Structure *16*, 115–124.

Fedorov, O., Huber, K., Eisenreich, A., Filippakopoulos, P., King, O., Bullock, A.N., Szklarczyk, D., Jensen, L.J., Fabbro, D., Trappe, J., et al. (2011). Specific CLK inhibitors from a novel chemotype for regulation of alternative splicing. Chem. Biol. *18*, 67–76.

Ferguson, M.W., and Joanen, T. (1982). Temperature of egg incubation determines sex in Alligator mississippiensis. Nature *296*, 850–853.

Gautherie, M., and Gros, C.M. (1980). Breast thermography and cancer risk prediction. Cancer *45*, 51–56.

Ge, C., Ye, J., Weber, C., Sun, W., Zhang, H., Zhou, Y., Cai, C., Qian, G., and Capel, B. (2018). The histone demethylase KDM6B regulates temperature-dependent sex determination in a turtle species. Science *360*, 645–648.

Georges, A., and Holleley, C.E. (2018). How does temperature determine sex? Science *360*, 601–602.

Ghosh, G., and Adams, J.A. (2011). Phosphorylation mechanism and structure of serine-arginine protein kinases. FEBS J. *278*, 587–597.

Goldammer, G., Neumann, A., Strauch, M., Müller-McNicoll, M., Heyd, F., and Preußner, M. (2018). Characterization of cis-acting elements that control oscillating alternative splicing. RNA Biol. *15*, 1081–1092.

Goldberg, J., Nairn, A.C., and Kuriyan, J. (1996). Structural basis for the autoinhibition of calcium/calmodulin-dependent protein kinase I. Cell *84*, 875–887.

Gong, J., Liu, J., Ronan, E.A., He, F., Cai, W., Fatima, M., Zhang, W., Lee, H., Li, Z., Kim, G.H., et al. (2019). A Cold-Sensing Receptor Encoded by a Glutamate Receptor Gene. Cell *178*, 1375–1386.e11.

Gotic, I., Omidi, S., Fleury-Olela, F., Molina, N., Naef, F., and Schibler, U. (2016). Temperature regulates splicing efficiency of the cold-inducible RNA-binding protein gene Cirbp. Genes Dev. *30*, 2005–2017.

Henzler-Wildman, K., and Kern, D. (2007). Dynamic personalities of proteins. Nature *450*, 964–972.

Hess, B. (2008). P-LINCS: A Parallel Linear Constraint Solver for Molecular Simulation. J. Chem. Theory Comput. *4*, 116–122.

Hess, B., Kutzner, C., van der Spoel, D., and Lindahl, E. (2008). GROMACS 4: Algorithms for Highly Efficient, Load-Balanced, and Scalable Molecular Simulation. J. Chem. Theory Comput. *4*, 435–447.

Hoekstra, M.M., Emmenegger, Y., Hubbard, J., and Franken, P. (2019). Cold-inducible RNA-binding protein (CIRBP) adjusts clock-gene expression and REM-sleep recovery following sleep deprivation. eLife *8*. Published online February 5, 2019. https://doi.org/10.7554/eLife.43400.

Horii, Y., Shiina, T., Uehara, S., Nomura, K., Shimaoka, H., Horii, K., and Shimizu, Y. (2019). Hypothermia induces changes in the alternative splicing pattern of cold-inducible RNA-binding protein transcripts in a non-hibernator, the mouse. Biomed. Res. (Aligarh) *40*, 153–161.

Humphrey, W., Dalke, A., and Schulten, K. (1996). VMD: visual molecular dynamics. J. Mol. Graph. *14*, 33–38, 27–28.

Hunter, J.D. (2007). Matplotlib: A 2D Graphics Environment. Comput. Sci. Eng. *9*, 90–95.

Huse, M., and Kuriyan, J. (2002). The conformational plasticity of protein kinases. Cell *109*, 275–282.

Isshiki, Y., Kohchi, Y., Iikura, H., Matsubara, Y., Asoh, K., Murata, T., Kohchi, M., Mizuguchi, E., Tsujii, S., Hattori, K., et al. (2011). Design and synthesis of novel allosteric MEK inhibitor CH4987655 as an orally available anticancer agent. Bioorg. Med. Chem. Lett. *21*, 1795–1801.

Johnson, L.N., Noble, M.E.M., and Owen, D.J. (1996). Active and inactive protein kinases: structural basis for regulation. Cell *85*, 149–158.

Jorgensen, W.L., Chandrasekhar, J., Madura, J.D., Impey, R.W., and Klein, M.L. (1983). Comparison of simple potential functions for simulating liquid water. J. Chem. Phys. *79*, 926–935.

Keil, G., Cummings, E., and de Magalhães, J.P. (2015). Being cool: how body temperature influences ageing and longevity. Biogerontology *16*, 383–397.

Keshwani, M.M., Hailey, K.L., Aubol, B.E., Fattet, L., McGlone, M.L., Jennings, P.A., and Adams, J.A. (2015). Nuclear protein kinase CLK1 uses a non-traditional docking mechanism to select physiological substrates. Biochem. J. *472*, 329–338.

Leuenberger, P., Ganscha, S., Kahraman, A., Cappelletti, V., Boersema, P.J., von Mering, C., Claassen, M., and Picotti, P. (2017). Cell-wide analysis of protein thermal unfolding reveals determinants of thermostability. Science *355*. Published online February 24, 2017. https://doi.org/10.1126/science.aai7825.

Liu, Y., Hu, W., Murakawa, Y., Yin, J., Wang, G., Landthaler, M., and Yan, J. (2013). Cold-induced RNA-binding proteins regulate circadian gene expression by controlling alternative polyadenylation. Sci. Rep. *3*, 2054.

Long, J.C., and Caceres, J.F. (2009). The SR protein family of splicing factors: master regulators of gene expression. Biochem. J. *417*, 15–27.

Lujan, D.A., Ochoa, J.L., and Hartley, R.S. (2018). Cold-inducible RNA binding protein in cancer and inflammation. Wiley Interdiscip. Rev. RNA *9*. Published online March 2018. https://doi.org/10.1002/wrna.1462.

Mallajosyula, S.S., Guvench, O., Hatcher, E., and Mackerell, A.D., Jr. (2012). CHARMM Additive All-Atom Force Field for Phosphate and Sulfate Linked to Carbohydrates. J. Chem. Theory Comput. *8*, 759–776.

Maslon, M.M., Heras, S.R., Bellora, N., Eyras, E., and Cáceres, J.F. (2014). The translational landscape of the splicing factor SRSF1 and its role in mitosis. eLife. . May 6, 2014. https://doi.org/10.7554/eLife.02028.

Morf, J., Rey, G., Schneider, K., Stratmann, M., Fujita, J., Naef, F., and Schibler, U. (2012). Cold-inducible RNA-binding protein modulates circadian gene expression posttranscriptionally. Science *338*, 379–383.

Müller-McNicoll, M., Botti, V., de Jesus Domingues, A.M., Brandl, H., Schwich, O.D., Steiner, M.C., Curk, T., Poser, I., Zarnack, K., and Neugebauer, K.M. (2016). SR proteins are NXF1 adaptors that link alternative RNA processing to mRNA export. Genes Dev. *30*, 553–566.

Ngo, J.C., Chakrabarti, S., Ding, J.H., Velazquez-Dones, A., Nolen, B., Aubol, B.E., Adams, J.A., Fu, X.D., and Ghosh, G. (2005). Interplay between SRPK and Clk/Sty kinases in phosphorylation of the splicing factor ASF/SF2 is regulated by a docking motif in ASF/SF2. Mol. Cell *20*, 77–89.

Ninomiya, K., Kataoka, N., and Hagiwara, M. (2011). Stress-responsive maturation of Clk1/4 pre-mRNAs promotes phosphorylation of SR splicing factor. J. Cell Biol. *195*, 27–40.

Nolen, B., Taylor, S., and Ghosh, G. (2004). Regulation of protein kinases; controlling activity through activation segment conformation. Mol. Cell *15*, 661–675.

Preußner, M., and Heyd, F. (2018). Temperature-controlled Rhythmic Gene Expression in Endothermic Mammals: All Diurnal Rhythms are Equal, but Some are Circadian. BioEssays *40*, e1700216.

Preußner, M., Wilhelmi, I., Schultz, A.S., Finkernagel, F., Michel, M., Möröy, T., and Heyd, F. (2014). Rhythmic U2af26 alternative splicing controls PERIOD1 stability and the circadian clock in mice. Mol. Cell *54*, 651–662.

Preußner, M., Goldammer, G., Neumann, A., Haltenhof, T., Rautenstrauch, P., Müller-McNicoll, M., and Heyd, F. (2017). Body Temperature Cycles Control Rhythmic Alternative Splicing in Mammals. Mol. Cell *67*, 433–446.

Qiang, X., Yang, W.L., Wu, R., Zhou, M., Jacob, A., Dong, W., Kuncewitch, M., Ji, Y., Yang, H., Wang, H., et al. (2013). Cold-inducible RNA-binding protein (CIRP) triggers inflammatory responses in hemorrhagic shock and sepsis. Nat. Med. *19*, 1489–1495.

Ran, F.A., Hsu, P.D., Wright, J., Agarwala, V., Scott, D.A., and Zhang, F. (2013). Genome engineering using the CRISPR-Cas9 system. Nat. Protoc. *8*, 2281–2308.

Refinetti, R., and Menaker, M. (1992). The circadian rhythm of body temperature. Physiol. Behav. *51*, 613–637.

Saini, C., Morf, J., Stratmann, M., Gos, P., and Schibler, U. (2012). Simulated body temperature rhythms reveal the phase-shifting behavior and plasticity of mammalian circadian oscillators. Genes Dev. *26*, 567–580.

Sali, A., and Blundell, T.L. (1993). Comparative protein modelling by satisfaction of spatial restraints. J. Mol. Biol. *234*, 779–815.

Schroeder, A.L., Metzger, K.J., Miller, A., and Rhen, T. (2016). A Novel Candidate Gene for Temperature-Dependent Sex Determination in the Common Snapping Turtle. Genetics *203*, 557–571.

Shalgi, R., Hurt, J.A., Lindquist, S., and Burge, C.B. (2014). Widespread inhibition of posttranscriptional splicing shapes the cellular transcriptome following heat shock. Cell Rep. *7*, 1362–1370.

Shin, C., Feng, Y., and Manley, J.L. (2004). Dephosphorylated SRp38 acts as a splicing repressor in response to heat shock. Nature *427*, 553–558.

Sterne-Weiler, T., Weatheritt, R.J., Best, A.J., Ha, K.C.H., and Blencowe, B.J. (2018). Efficient and Accurate Quantitative Profiling of Alternative Splicing Patterns of Any Complexity on a Laptop. Mol. Cell *72*, 187–200.

Studier, F.W. (2005). Protein production by auto-induction in high density shaking cultures. Protein Expr. Purif. *41*, 207–234.

Tan, P.L., and Katsanis, N. (2009). Thermosensory and mechanosensory perception in human genetic disease. Hum. Mol. Genet. *18* (R2), R146–R155.

Taylor, S.S., and Radzio-Andzelm, E. (1994). Three protein kinase structures define a common motif. Structure *2*, 345–355.

Thomas, T.M., and Scopes, R.K. (1998). The effects of temperature on the kinetics and stability of mesophilic and thermophilic 3-phosphoglycerate kinases. Biochem. J. *330*, 1087–1095.

Thompson, M.C., Barad, B.A., Wolff, A.M., Sun Cho, H., Schotte, F., Schwarz, D.M.C., Anfinrud, P., and Fraser, J.S. (2019). Temperature-jump solution X-ray scattering reveals distinct motions in a dynamic enzyme. Nat. Chem. *11*, 1058–1066.

Van Der Spoel, D., Lindahl, E., Hess, B., Groenhof, G., Mark, A.E., and Berendsen, H.J. (2005). GROMACS: fast, flexible, and free. J. Comput. Chem. *26*, 1701–1718.

Walt, S.d., Colbert, S.C., and Varoquaux, G. (2011). The NumPy Array: A Structure for Efficient Numerical Computation. Comput. Sci. Eng. *13*, 22–30.

Weik, M., and Colletier, J.P. (2010). Temperature-dependent macromolecular X-ray crystallography. Acta Crystallogr. D Biol. Crystallogr. *66*, 437–446.

Wetsel, W.C. (2011). Sensing hot and cold with TRP channels. Int. J. Hyperthermia *27*, 388–398.

Wong, R.W., Balachandran, A., Ostrowski, M.A., and Cochrane, A. (2013). Digoxin suppresses HIV-1 replication by altering viral RNA processing. PLoS Pathog. *9*, e1003241.

Yang, H., Guranovic, V., Dutta, S., Feng, Z., Berman, H.M., and Westbrook, J.D. (2004). Automated and accurate deposition of structures solved by X-ray diffraction to the Protein Data Bank. Acta Crystallogr. D Biol. Crystallogr. *60*, 1833–1839.

Zhong, X.-Y., Wang, P., Han, J., Rosenfeld, M.G., and Fu, X.-D. (2009). SR proteins in vertical integration of gene expression from transcription to RNA processing to translation. Mol. Cell *35*, 1–10.

Zhou, Z., and Fu, X.D. (2013). Regulation of splicing by SR proteins and SR protein-specific kinases. Chromosoma *122*, 191–207.

STAR★METHODS

KEY RESOURCES TABLE

REAGENT or RESOURCE	SOURCE	IDENTIFIER
Antibodies		
Rabbit polyclonal anti DYKDDDK Tag Antibody (FLAG)	Cell Signaling Technology	Cat# 2368S; RRID:AB_2217020
Mouse monoclonal anti HNRNPL (4D11) Antibody	Santa Cruz Biotechnology	Cat# sc-32317; RRID:AB_627736
Mouse monoclonal anti GAPDH Antibody (GT239)	GeneTex	Cat# GTX627408; RRID:AB_11174761
Mouse monoclonal anti SR Antibody (1H4)	Merck	Cat# MABE50; RRID:AB_10807429
Chemicals, Peptides, and Recombinant Proteins		
γ-^{32}P-ATP	Hartmann Analytic	Cat# SRP-501
TG-003	Sigma Aldrich	Cat# T5575-5MG
Deposited Data		
Mendeley Data	Unprocessed images of this study	https://doi.org/10.17632/5mt4vjxztr.1
GEO accession number	This paper	GSE143872
PDB: 6TW2	PDB: 2VAG	NA
Experimental Models: Cell Lines		
Homo sapiens Hek293T cell line	see STAR Methods	RRID:CVCL_0063
Trachemys scripta elegans SKM-R	see STAR Methods	CCLV-RIE 482
Terrapene carolina TH-1	see STAR Methods	CCLV-RIE 1131
Experimental Models: Organisms/Strains		
C57BL/6 wildtype mice	NA	NA
E. coli BL21 Rosetta 2	NA	NA
E. coli BL21 (DE3)	NA	NA
Oligonucleotides		
sequences of oligonucleotides are available upon request	This study	NA
Recombinant DNA		
pGex 6P1	Merck	Cat# GE28-9546-48
PX459	Kindly provided by Stefan Mundlos	Ran et al., 2013
pEGFP-N3	Clontech	Cat# 6080-1
Software and Algorithms		
ImageQuantTL	GE Healthcare Life Sciences	29000737
Whippet v0.11	Sterne-Weiler et al., 2018	https://github.com/timbitz/Whippet.jl
PHENIX	Adams et al., 2010; Afonine et al., 2012	https://www.phenix-online.org/
COOT v0.8.2	Emsley et al., 2010	https://www2.mrc-lmb.cam.ac.uk/personal/pemsley/coot/
PyMol	Schrödinger	https://pymol.org/2/
Gromacs v4.6.7	(Hess, 2008; Van Der Spoel et al., 2005	
matplotlib	Hunter, 2007	

LEAD CONTACT AND MATERIALS AVAILABILITY

Please contact F.H. (florian.heyd@fu-berlin.de) for reagents and resources generated in this study.

EXPERIMENTAL MODEL AND SUBJECT DETAILS

Mouse maintenance

All animal experiments were performed with C57BL/6 mice in accordance with institutional and governmental recommendations and laws (permission T 0311/13). Mice were kept under 12-hour light-dark conditions. To isolate primary mouse hepatocytes, liver was perfused with PBS and digested using Collagen digestion solution. Liver was transferred into a Petri dish and cells were liberated by mechanical force. Cells were washed three time with Williams Medium E and 10% FCS and plated.

Tissue culture cells

HEK293T cells are maintained in liquid nitrogen and early passage aliquots are thawed periodically. Cell morphology is routinely assessed, to rule out mycoplasma contamination this is monthly checked using a PCR-based assay. HEK293T were maintained in DMEM medium containing 10% FBS and Pen/Strep (Invitrogen) at the indicated temperatures.

METHOD DETAILS

Cloning and Protein purifications

For overexpression of CLK1-4 f.l. and KD, inserts were amplified from mouse or human cDNA and cloned into the pGEX-6P1 bacterial expression vector. Ts/Tc CLK1f.l., amCLK4 f.l. or KD or *D. melanogaster* darker of apricot (DOA) KD were amplified from turtle RNA or ordered as a synthetic gene (MWG), respectively. A DNA fragment encoding the substrate GST-GRSRSRSRS was cloned into pGEX-6P1 by synthetic oligonucleotides, harboring restriction sites. The expression construct for human SRPK1 was kindly provided by Gourisankar Ghosh (UCSD). For activation segment hybrid mutants, SRPK1 was shuttled into pGEX-6P1. Hybrid mutants and point mutants were generated by 2-step PCRs and conventional cloning. All constructs were validated by sequencing. Constructs were expressed in the *Escherichia coli* strain BL21 (DE3) by induction with 0.2 mM IPTG at 18°C overnight. Cells were lysed by sonication and cleared by centrifugation, followed by GSH-Sepharose affinity chromatography. The protein was eluted with 3 column volumes (CVs) of lysis buffer (for CLK1 f.l. and KD: 50 mM HEPES/NaOH (pH 7.5), 500 mM NaCl, 5% (v/v) glycerol, 50 mM L-glutamic acid, 50 mM L-arginine; for CLK4 f.l. and KD and the RS containing substrate: 50 mM Tris/HCl (pH 8.4), 300 mM NaCl, 1 mM DTT) supplemented with 20 mM gluthathione, followed by dialysis in 3 l lysis Buffer. F.l. proteins and SR-substrate were used after dialysis. Where indicated, CLK1/4 KD was cleaved with Prescission protease, recycled over GSH-beads and further purified by size exclusion chromatography (S75 10/300). Aliquots were flash frozen in liquid nitrogen and stored at −80°C until use. His-tagged SRPK1 (used in Figure 2) was expressed in *E. coli* BL21 Rosetta 2 cells in ZYM auto-induction medium (Studier, 2005). Cells were lysed by sonication (Sonopuls HD 3100, Bandelin) in buffer (400 mM NaCl, 40 mM Tris/HCl, pH 7.5, 5% (v/v) glycerol, 1 mM DTT) and purified by Ni^{2+}-NTA affinity chromatography (Macherey Nagel) and anion exchange chromatography (High Trap QXL, GE Healthcare) according to the manufacturer's protocol, and a final purification was done by size exclusion chromatography (SEC) on Superdex S200 10/300 Increase columns (GE Healthcare) in SEC buffer (200 mM NaCl, 20 mM Tris/HCl, pH 7.5, 5% (v/v) glycerol, 1 mM DTT). Purified proteins were concentrated to 10-20 mg/ml and flash frozen in liquid nitrogen.

Kinase assay

Reaction mixtures contained the respective kinase, GST-SR substrate, kinase buffer (10X: 700 mM Tris/HCl (pH 7.6), 100 mM $MgCl_2$, 50 mM DTT) and ~2 mM [γ-^{32}P]ATP (~0.025 Ci mmol^{-1}) in a final volume of 15 µl. Proteins were affinity purified as described above (for one assay, an OD equivalent of 80 from bacteria culture was used), but not eluted. Bead slurry with bound kinases and substrate were mixed 1:1 and washed 5 times with lysis buffer. After the final wash, 14 µl 1X kinase buffer was added. Reaction mixtures were pre-incubated without [γ-^{32}P]ATP for 20 min at indicated temperatures, then 1 µl [γ-^{32}P]ATP (2 mM final concentration) was added followed by another 5 min incubation step (for Figure 5B CLK wt KD and CLK mut KD 1 hour). For temperature shift experiments, samples were pre-incubated at indicated temperatures for 20 min. After adding [γ-^{32}P]ATP, samples were shifted back to colder temperatures and incubated for 1-60 min. Reactions were stopped by adding 6X SDS-loading dye, samples were heated to 95°C for 5 min and analyzed on a 12% or 15% SDS-PAGE. Gels were stained with Coomassie and imaged. Afterward, they were transferred onto filter papers and dried for 1 hour in a gel drier. The dried gels were exposed to phosphoscreens overnight. Detection was carried out with a Phosphoimager and ImageQuant TL software.

Cell culture, RNA extraction, RT-PCRs, Transfection and western blot

HEK293 cells were cultured in DMEM High glucose (Biowest) containing 10% FCS (Biochrom) and 1% Penicillin/Streptomycin (Biowest). Temperature shifts and RT-PCRs were performed as previously described (Preußner et al., 2017). Briefly, RNA was extracted using RNATri (Bio&Sell) and 1 µg RNA was used in a gene-specific RT-reaction. Low-cycle PCR with a ^{32}P-labeled forward primer was performed, products were separated by denaturing PAGE and quantified using a Phosphoimager and ImageQuantTL software. Results of endogenous AS represent the mean value of at least three independent experiments with the according SD *T. scripta* and *T. carolina* cell lines were obtained from the Friedrich-Loeffler-Institut (Greifswald, Germany). Cell culture was performed at 26°C in a humidified atmosphere with 2.5% CO_2. *T. scripta* cell line (derived from spleen of a juvenile) was cultured w/o antibiotics in a 1:1 mixture of Ham's F-12 Nutrient Mix (Thermo Scientific) and Iscove's Modified Dulbecco's Medium (Thermo Scientific) with 10% (v/v)

fetal bovine serum. The *T. carolina* cell line (explant culture from heart) was cultured in DMEM High glucose (Biowest). For temperature shift experiments cells were either kept at 26°C or 31.5°C for 4 h.

For qRT-PCR, gene-specific primers for *Gapdh* and a reverse primer within intron 15 and a reverse primer within exon 16 of *Jarid2* (for intron retention in turtle cell lines) were combined in one RT reaction. qPCR was then performed in 96 well format using the ABsolute QPCR SYBR Green Mix (Thermo Fisher) on a Stratagene Mx3000P instrument. qPCRs were performed in technical duplicates, mean values were used to normalize expression to mRNA of *Gapdh* (ΔCT) and Δ(ΔCT)s were calculated for different conditions. For intron retention mean values of intron products were normalized to products of spliced mRNA using primers in flanking exons. Significance was calculated by Student's unpaired t test and significance is indicated: *$p < 0.05$, **$p < 0.01$, ***$p < 0.001$. Primer sequences are available upon request.

For overexpression experiments, $1.5x10^5$ HEK293 cells in a 12 well plate were transfected with 0.8 μg expression vectors for Flag-tagged CLK1 and CLK1 H343Q. 48 hours after transfection, cells were incubated at 39°C for 12 hours. Samples were then incubated for 6 hours at either 39°C or 35°C and RNA was prepared and analyzed as above.

SDS-PAGE and immunoblotting were performed according to standard protocols. Briefly, to extract proteins, cells were washed with PBS and lysed with 1x RIPA buffer (10 mM Tris/HCl (pH 8.0), 1% (v/v) NP40, 4 mM EDTA, 200 mM NaCl, 5 mg/ml sodium deoxycholate) containing protease and phosphatase inhibitors. Phosphorylation of SR-Proteins was analyzed by SDS-PAGE, blotting to a PVDF membrane, and using the Anti-Phosphoepitope SR protein antibody 1H4 (Merck, MABE50) and against GAPDH (GT239, GeneTex) as loading control. Expression of Flag-tagged CLK1 and CLK1 H343Q was analyzed by SDS-PAGE, blotting to a PVDF membrane, and using antibodies against the Flag-Tag (Cell Signaling, 2368) and against GAPDH (GT239, GeneTex) as loading control.

Investigation of AS and gene expression by RNA sequencing

To identify CLK-dependent and temperature-regulated AS in human cells, confluent HEK293 cells were incubated at 39°C for 12 hours. Cells were then treated with 50 μM TG003 (or DMSO as solvent control) and after further 30 minutes at 39°C, samples were incubated for 6 hours at either 39°C or 35°C. RNA was extracted using RNATri (Bio&Sell) followed by DNaseI digestion. Sequencing libraries were analyzed on a HiSeq4000 instrument yielding ~50 million paired-end 150-bp reads per replicate and condition. Reads were aligned to the hg38 genome and splicing patterns as well as transcripts per million (tpm) values were determined using Whippet version 0.11 (Sterne-Weiler et al., 2018). Events with a minimum PSI difference of 0.15 and a probability above 0.9 between the two temperatures in DMSO control were further investigated. For gene expression, genes were considered temperature-dependent in DMSO when first tpm values are > 5 in all 12 samples, second the Δtpm between the three DMSO35 and DMSO39 is > 5 (with the same directionality and a fold change of at least 1.2), and finally the mean fold-change is > 1.3 between DMSO35 and DMSO39. Downstream analyses were performed using Python2 (numpy, (Walt et al., 2011)), Matplotlib (data visualization, (Hunter, 2007)) or GraphPad Prism 7.05.

Generation of CRISPR-Cas9 edited cells and analysis of Cirbp expression

For genome-engineering in HEK293 cells, sequences flanking exon 7b and 8 of *Cirbp* were analyzed for sgRNA candidates *in silico* using the Benchling tool. Upstream and downstream a pair of oligonucleotides for the highest ranked candidate sgRNA (Ran et al., 2013) was synthesized and subcloned into the PX459 vector (kindly provided by Stefan Mundlos). sgRNA sequences: upstream: 5′-ctagcctgagaccttcctag; downstream: 5′-cgcacgagtaggacccgaca. Cells were transfected in 6-well plates using Rotifect following the manufacturer's protocol. 48 hours after transfection, the transfected cells were selected with 1 μg/ml puromycin and clonal cell lines were isolated by dilution (Ran et al., 2013). Genomic DNA was extracted using DNA extraction buffer (200 mM Tris/HCl pH 8.3, 500 mM KCl, 5 mM $MgCl_2$, 0.1% gelatin in H_2O) and a PCR was performed to confirm the exon knockout on DNA level. In promising clones the exon knockout was additionally confirmed after RNA isolation by splicing sensitive PCR using one forward primer in exon 6 and two reverse primers in exon 7a or exon 7b, respectively. *Cirbp* total expression levels were investigated by RT-qPCR as described above (qPCR primers detect both the E7a and E7b isoforms simultaneously).

To analyze *Cirbp* AS and gene expression in mice, we prepared primary hepatocytes from adult mice and incubated them at the indicated temperatures and additionally re-investigated RNA from livers from young mice from different ambient temperatures, as previously described (Preußner et al., 2017). Due to primer design the exon 7b product is larger than the 7a product in human and smaller in mouse.

To investigate *Cirbp* AS in RNA-Seq data we used the –sam tag of Whippet version 0.11 (Sterne-Weiler et al., 2018) to create sam files. These were transferred to bam files, sorted and indexed using samtools. Sashimi blots were created using IGV genome browser, PSI values were manually determined using the junction reads to exons 7a and 7b. Conservation scores across 100 vertebrates are from the '100 vertebrates Basewise Conservation by PhyloP' track from the UCSC Genome browser.

Molecular Dynamics Simulation

The SRPK1 protein was modeled based on crystal structure PDB: 1WBP (Ngo et al., 2005). A large loop of residues 238-476 missing in the crystal structure was not modeled. Instead, the first and last resolved residue bordering this loop, 237 and 477, respectively, were capped by neutral termini and positionally restrained. The peptide substrate present in the crystal structure was removed and the ADP molecule was changed to ATP. The missing coordinates of the γ-phosphate and the Mg^{2+} ion were taken from the crystal

structure of another kinase-ATP-Mg^{2+} complex, PDB: 3OS3 (Isshiki et al., 2011). The KD of the CLK1 protein was modeled based on the crystal structure PDB: 1Z57 (Bullock et al., 2009). Residues 307 to 310 and 483 to 494 missing in the crystal structure were modeled by using the Modeller9.19 tool kit (Sali and Blundell, 1993). The 10Z-Hymenialdisine inhibitor bound in the crystal structure was replaced by ATP and a Mg^{2+} ion taken from, and similarly placed as in our SRPK1 model (after superimposing the active sites of the two proteins). All titratable groups were kept in their standard protonation states. The proteins, ATP, and Mg^{2+} ion were described by the charmm36 force field (Best et al., 2012; Mallajosyula et al., 2012). The protein-ATP-Mg^{2+} models were immersed in a periodic cubic box (side length of 11 nm) with TIP3P water (Jorgensen et al., 1983) (~130,000 atoms in total). Van der Waals and short-range electrostatic interactions were truncated after 1.4 nm, long-range electrostatic interactions were treated with the particle mesh Ewald method and a 0.16 nm Fourier grid spacing. After an initial minimization, a first equilibration at 300 K for 1 ns with positional restraints on all heavy atoms was performed, followed by another round of equilibrations, again at 300 K and for 1 ns, with positional restraints only on the ATP molecule and the Mg^{2+} ion. After equilibration, three individual 500-ns production simulations were performed for each model system, starting with different initial velocities, at either 293 K or 313 K. All covalent bonds to hydrogen atoms were constrained by the LINCS algorithm (Hess et al., 2008), allowing an integration time step of 2 fs. The V-rescale thermostat (Bussi et al., 2007) was employed to control temperature at 293 K or 313 K. All simulations were performed with the gromacs package, version 4.6.7 (Hess, 2008; Van Der Spoel et al., 2005). Analyses were carried out with tools provided by the gromacs package. Only the last 400 ns of each simulation were analyzed, considering the first 100 ns as further equilibration time. Values reported are averages over the three individual simulations of each model system and errors are estimated as SDs. Graphics were prepared by using VMD (Humphrey et al., 1996) and the python library matplotlib (Hunter, 2007).

The H344A mutant was generated from the equilibrated wild-type structures by *in silico* replacing H344 with alanine. After re-equilibration at 313 K, the mutant model was subjected to one 200 ns long production run with the same settings as for the simulations of the wild-type systems.

CD-spectroscopy

CD-spectroscopy was performed with 0.015 mg/ml hCLK1 KD in kinase buffer as used for *in vitro* kinase assays in a JASCO J-715 Spectropolarimeter. CD spectra were recorded from 200 to 250 nm at 25°C, 34°C and 38°C after an initial incubation at the given temperatures for 5 min. For each temperature 3 spectra were recorded and averaged.

Crystallographic procedures

The structure factor amplitudes and coordinates of PDB entry 2VAG (Fedorov et al., 2011) were downloaded from the ProteinDataBank. In the first round of refinement a simulated annealing protocol as implemented in PHENIX (Adams et al., 2010; Afonine et al., 2012), was performed. The resulting electron densities clearly revealed a second conformation of the activation segment (Figure S5A). Manual model building was performed with COOT (Emsley et al., 2010). Further maximum likelihood refinement cycles were performed with PHENIX including TLS refinement and occupancy refinement. Model quality was evaluated with MolProbity (Chen et al., 2010) and the JCSG validation server (Yang et al., 2004). The kinase substrate was superimposed on the CLK structures (PDB: 1Z57; PDB: 6TW2) using the crystal structure of the catalytic subunit of the cAMP-dependent protein kinase complexed with a substrate peptide (PDB: 1JBP) as template. Figures were generated with PyMol (Schrödinger).

QUANTIFICATION AND STATISTICAL ANALYSIS

All data are represented as mean ± standard deviation (SD). Figure legends contain information on independent biological replicates and statistical tests used.

DATA AND CODE AVAILABILITY

Full gel images and raw data files are deposited as Mendeley Data (https://doi.org/10.17632/5mt4vjxztr.1). Coordinates for the re-refined structure and structure factors of human CLK1 have been deposited in the RCSB Protein Data Bank (https://www.rcsb.org/) with accession code 6TW2. RNA sequencing data are available under GEO #GSE143872.

Molecular Cell, Volume *78*

Supplemental Information

A Conserved Kinase-Based Body-Temperature Sensor Globally Controls Alternative Splicing and Gene Expression

Tom Haltenhof, Ana Kotte, Francesca De Bortoli, Samira Schiefer, Stefan Meinke, Ann-Kathrin Emmerichs, Kristina Katrin Petermann, Bernd Timmermann, Petra Imhof, Andreas Franz, Bernhard Loll, Markus C. Wahl, Marco Preußner, and Florian Heyd

Supplemental information

A conserved kinase-based body temperature sensor globally controls alternative splicing and gene expression

Tom Haltenhof[1], Ana Kotte[1], Francesca De Bortoli[1], Samira Schiefer[1], Stefan Meinke[1], Ann-Kathrin Emmerichs[1], Kristina Katrin Petermann[1], Bernd Timmermann[2], Petra Imhof[3], Andreas Franz[1,4], Bernhard Loll[4], Markus C. Wahl[4,5], Marco Preußner[1], Florian Heyd[1*]

[1]Freie Universität Berlin, Institute of Chemistry and Biochemistry, Laboratory of RNA Biochemistry, Takustrasse 6, 14195 Berlin, Germany.

[2]Sequencing Core Facility, Max-Planck-Institute for Molecular Genetics, Ihnestraße 63-73, Berlin 14195, Germany

[3]Freie Universität Berlin, Institute of Theoretical Physics, Arnimallee 14, 14195 Berlin, Germany.

[4]Freie Universität Berlin, Institute of Chemistry and Biochemistry, Laboratory of Structural Biochemistry, Takustrasse 6, 14195 Berlin, Germany.

[5]Helmholtz-Zentrum Berlin für Materialien und Energie, Macromolecular Crystallography, Albert-Einstein-Straße 15, 12489 Berlin, Germany

[*]Corresponding author / lead contact:

florian.heyd@fu-berlin.de

Phone: +49 30 83862938

FAX: +49 30 838-4-62938

Haltenhof et al., Supplemental table

Table S4. Model refinement statistics. For data collection statistics, please see the original publication by Fedorov *et al.* (Fedorov et al., 2011) and the related PDB ID 2VAG. (Related to Figure 5)

Refinement	
PDB ID	6TW2
Resolution range [Å][a]	30.00 - 1.80 (1.85 - 1.80)
Reflections [a]	
Number	36956 (2666)
Test Set (5.1 %)	1887 (154)
R_{work}	18.3 (33.1)
R_{free}	22.3 (36.5)
Contents of the Asymmetric Unit	
Protein copy, Residues, Atoms	1, 334, 3019
Ligand, atoms	1, 22
Water, Molecules	216
Mean Temperature factors [Å^2][b]	
All Atoms	35.7
Macromolecules	39.9
Ligands	27.1
Water Oxygens	39.0
RMSD from Target Geometry	
Bond Lengths [Å]	0.008
Bond Angles [°]	0.929
Validation Statistics [c]	
Ramachandran Plot	
Residues in Allowed Regions [%]	2.2
Residues in Favored Regions [%]	97.9
MOLPROBITY score [d]	1.35
MOLPROBITY Clashscore [d]	3.7

[a] data for the highest resolution shell in parenthesis
[b] calculated with PHENIX (Adams et al, 2010)
[c] calculated with MOLPROBITY (Chen et al, 2010)
[d] Clashscore is the number of serious steric overlaps (> 0.4) per 1,000 atoms.

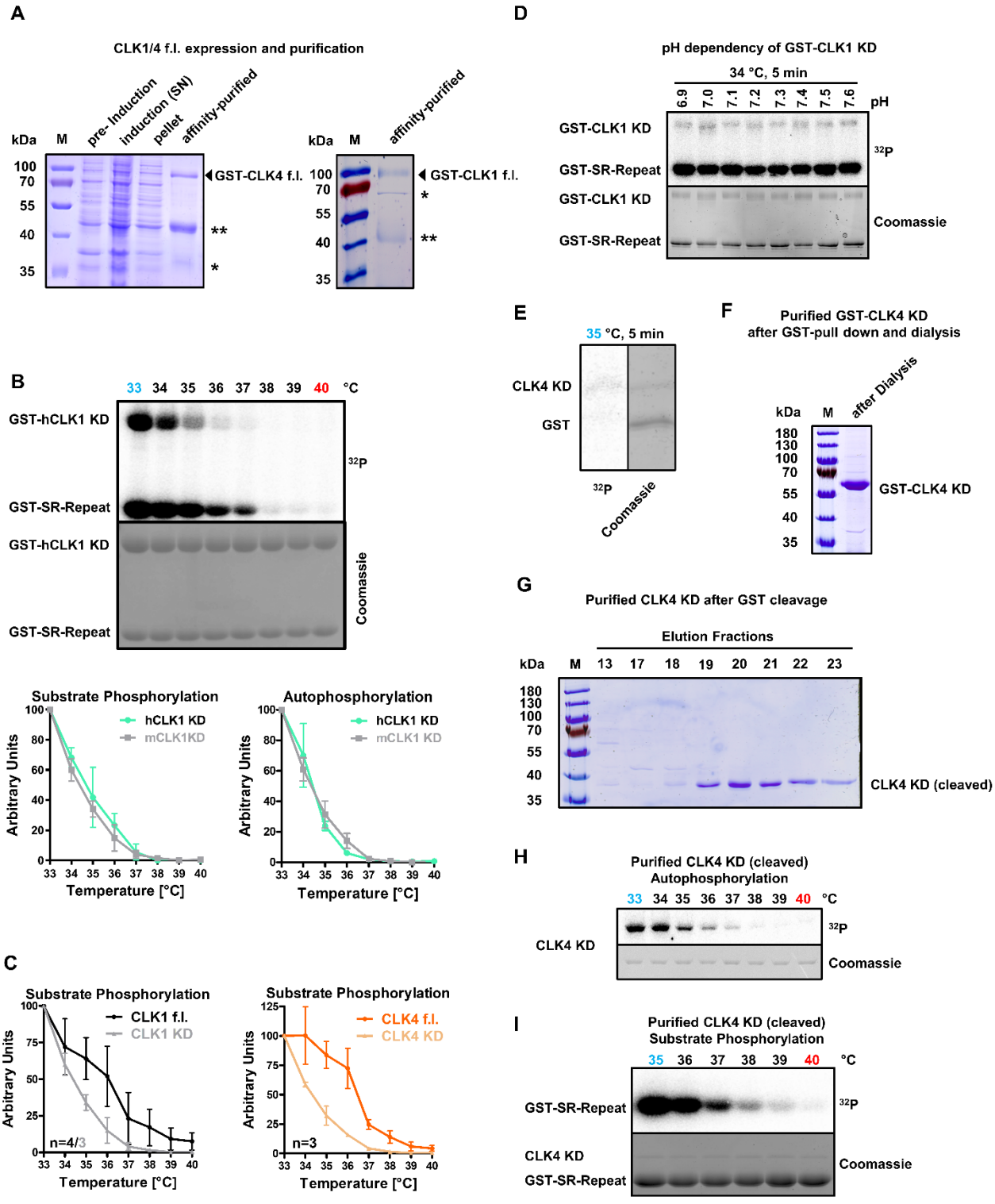

Figure S1. The activity of the CLK1/4 kinase domain is controlled by changes in the physiologically relevant temperature range (related to Figure 1)

(A) Purification of f.l. GST-CLK1/4. Coomassie-stained gels after purification are shown. Asterisks indicate degradation products. ** likely represents an N-terminally extended kinase domain, resulting from loss of the GST-tag with most of the unstructured N-terminus.

(B) Human (h) and mouse (m) CLK1 (91% identity, CLK4s are 97% identical) show identical temperature response curves. For hCLK1 KD a representative gel is shown. On the right, quantifications of substrate and autophosphorylation relative to mCLK1 kinase domain (from Figure 1) are shown (n=3, mean +/- SD).
(C) The CLK1/4 N-terminus shifts the temperature optimum. Comparison of the temperature response profiles of the f.l. kinase or the kinase domain lacking the N-terminus for mouse CLK1 (left) and CLK4 (right). Data from Figure 1.
(D) CLK1/4 kinase activity is not pH-dependent. To rule out secondary effects of temperature-mediated differences in pH, we confirmed lack of pH sensitivity of CLK1 kinase domain activity at 34°C in the pH range between 6.9 and 7.6.
(E) CLK4 specifically phosphorylates SR peptides. To rule out unspecific phosphorylation of GST, we incubated CLK4 kinase domain with a large excess of GST. In contrast to autophosphorylation, we did not observe any phosphorylation of GST alone.
(F) Coomassie-stained gel showing essentially pure GST-CLK4 kinase domain.
(G) Coomassie-stained gel showing purified CLK4 kinase domain after cleavage of GST.
(H, I) Purified CLK4 kinase domain – after cleavage of the GST-tag – shows temperature-dependent autophosphorylation (H) and substrate phosphorylation (I). Due to the similar size and stronger signal for substrate phosphorylation, autophosphorylation is not visible in (I). These controls validate the use of GST-tagged proteins for *in vitro* kinase assays.

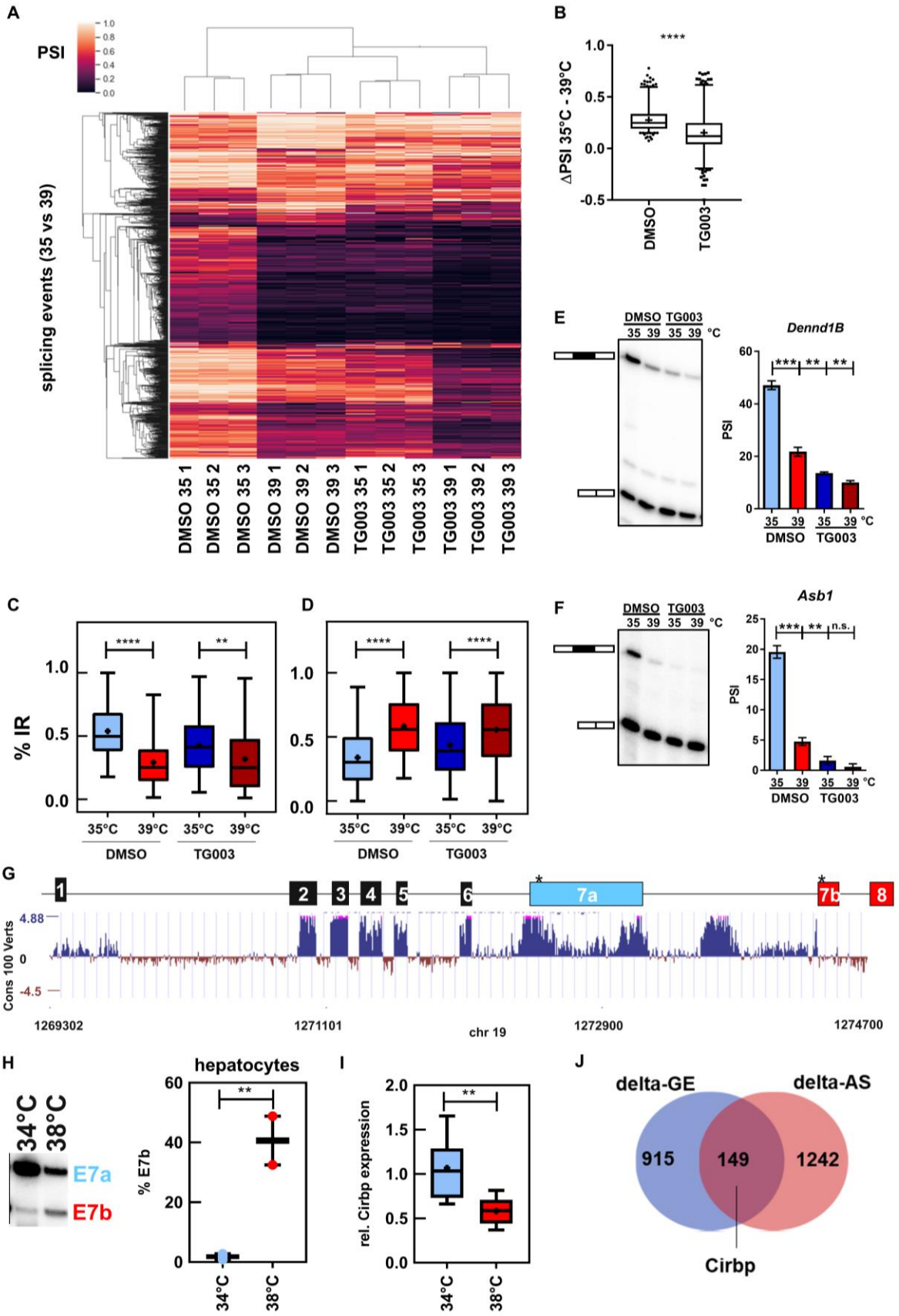

Figure legend on the next page

Figure S2. CLK activity controls body temperature-dependent alternative splicing and gene expression (related to Figure 3 and Figure 4)

(A) Unsupervised clustering of percent spliced in values for temperature-dependent exons presented in Figure 3C. Note the high similarity of the triplicate samples and the clear clustering of DMSO 39°C and TG003 35°C samples.

(B) Box-Whisker-Plots of ΔPSI values of skipped exon events as presented in Figure 3D. The line represents the median ΔPSI, circle represents mean ΔPSI (mean ΔPSI DMSO 0.27; mean ΔPSI TG003 0.15). Statistical significance was determined by unpaired t-test (****p<0.0001).

(C, D) Box-Whisker-Plots of intron retention (IR) events with higher IR at 35°C (C, n=101) or at 39°C (D, n=531). Note the reduced ΔPSI in TG003-treated samples. Statistical significance was determined by 1-way ANOVA (Tukey's multiple comparisons test, **p<0.01, ****p<$1x10^{-15}$).

(E-F) Representative gels and quantifications for additional splicing targets, *Dennd1b* (E) and *Asb1* (F). Statistical significance was determined by unpaired t-test.

(G) Evolutionary conservation across the whole *Cirbp* gene locus as shown in Figure 4C. Top: Exon/Intron structure of the whole *Cirbp* pre-mRNA. Exons are depicted by boxes, introns by lines, the asterisks indicate stop codons. Cold-preferred inclusion of exon 7a is indicated in blue, warm-preferred usage of exons 7b and 8 in red. Below the basewise comparison across 100 vertebrates by PhyloP track from the UCSC genome browser is shown. Values above zero show high conservation. Note that sequences downstream of exon 7a and at the 3' splice site of exon7b are as conserved as exonic protein coding sequences.

(H, I) *Cirbp* splicing (H) and gene expression (I) in mouse hepatocytes. Purified primary hepatocytes were incubated at 34 or 38°C. After 12 hours the temperature was switched and after further 8 hours *Cirbp* AS was investigated by radioactive RT-PCR (H). We used one forward primer in exon 6 and two reverse primers in exon 7a or exon 7b, respectively. Due to primer design the exon 7b product is larger in human and smaller in mouse than the 7a product. A representative gel is shown on the left and quantification of E7b inclusion is shown on the right (n>2, unpaired t-test derived p-value **p<0.01). Gene expression was analyzed by qRT-PCR and is shown normalized to *Gapdh* (C, n=8, unpaired t-test derived p-value **p<0.01).

(J) Overlap of genes with temperature-dependent gene expression (delta-GE) and temperature-dependent alternative splicing (delta-AS). Note that *Cirbp* was identified as a gene with temperature-dependent gene expression and AS.

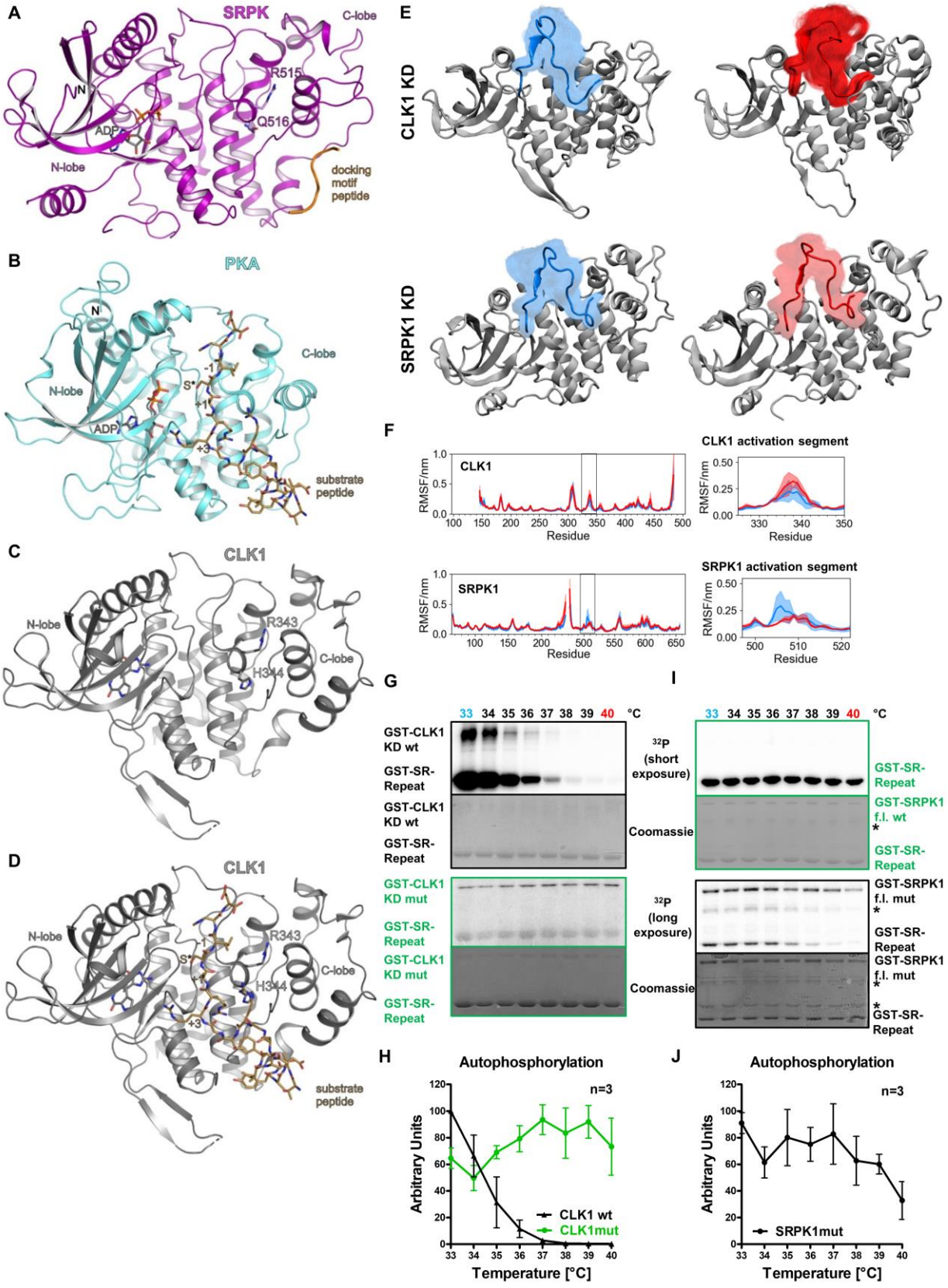

Figure S3. Temperature-sensitivity of CLK activity is mediated through the activation segment (related to Figure 5)

(A-D) Overall structures and superpositions of SRPK, PKA, as well as CLK1. (A) Structure of SRPK bound to ADP and a docking motif peptide (PDB ID 1WBP). Activation segment residues R515 and Q516 (subjected to mutagenesis) are shown in stick representation. (B) Structure of catalytic subunit of cAMP-dependent PKA complexed with ADP and a substrate peptide (PDB ID 1JBP). The ADP (gray) and the peptide is shown in stick representation (light brown). (C) Structure of CLK1 bound to 10Z-Hymenialdisine inhibitor (PDB ID 1Z57). Activation segment residues (R343 and H344) subjected to mutagenesis and the inhibitor are shown in stick representation. (D) A superposition of CLK1 and the PKA substrate to locate the potential substrate binding site within the CLK active center; the target serine is indicated as S*. The inhibitor is shown in stick representation.

(E) Temperature-dependent molecular dynamics (MD) simulations were performed with the kinase domains of CLK1 (top, PDB: 1Z57) and SRPK1 (bottom, PDB: 1WBP) at 20°C (blue) and at 40°C (red). These temperatures represent maximal and completely lost activity, see Figure 2A. No global structural differences are visible comparing 20°C and 40°C. The shaded areas represent the volumes in which the activation segments were observed during the MD simulations. Note that the CLK1 activation segment (top) shows higher flexibility (larger shaded area) at 40°C.

(F) Flexibility of kinase domains of CLK1 (top) and SRPK1 (bottom), quantified as root mean square fluctuation (RMSF) of the C-alpha Atoms at 20°C and 40°C. Activation segments are shown boxed on the left and in detail on the right. Heat leads to a higher flexibility of a central part of the CLK1 activation segment (top) but not SRPK1, which shows rather reduced flexibility at higher temperatures (bottom, residues between 238-476 were not defined in the available crystal structures).

(G, H) Introducing the SRPK1 activation segment into the CLK1 kinase domain abolishes temperature sensitivity. CLK1 kinase domain wt (black) and a mutant (mut) containing the SRPK1 activation segment (green) were investigated as in Figure 1B (longer incubation time, see methods). Representative gel images are shown in (G). Quantification of substrate phosphorylation is shown in Figure 5B. The quantification in (H) illustrates that the mutant with the SRPK1 activation segment in the CLK1 kinase domain lost temperature-sensitive autophosphorylation (n=3, mean +/- SD).

(I, J) Introducing the CLK1 activation segment into SRPK1 creates temperature sensitivity. SRPK1 wt (green) and a mutant containing the CLK1/4 activation segment (black) were investigated as in Figure 1B. The asterisks indicate SRPK1 degradation products. Representative gel images are shown in (I). Quantification of substrate phosphorylation is shown in Figure 5B. The quantification in (J) illustrates that the SRPK mutant bearing the CLK activation segment gained temperature-sensitive autophosphorylation (n=3, mean +/- SD). Due to lower kinase activity of the mutant kinases a longer exposure of the gels is shown.

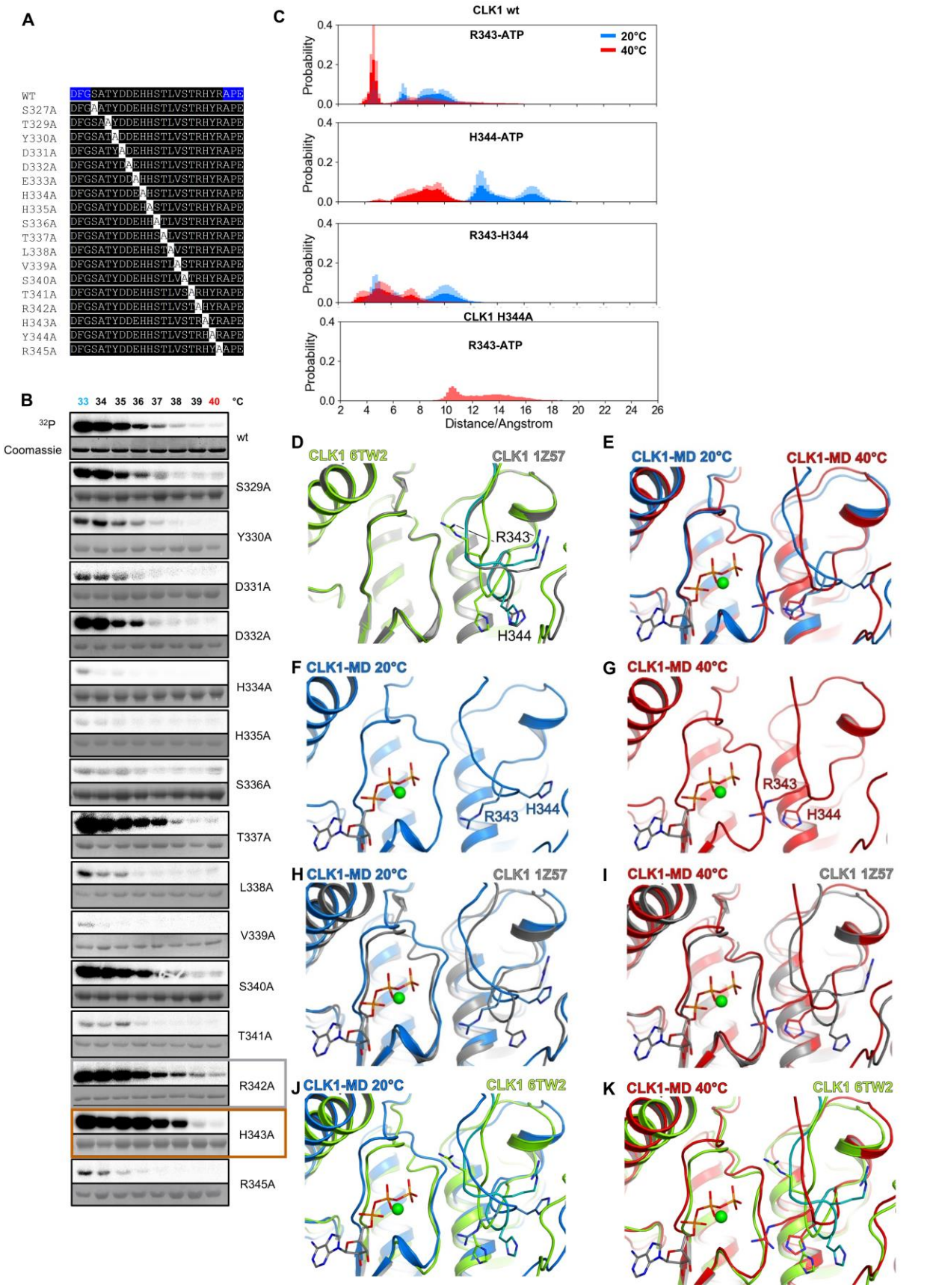

Figure legend on the next page

Figure S4. Temperature-sensitivity of CLK activity is mediated through specific residues in the activation segment (related to Figure 5)

(A) Schematics of the alanine scan of the CLK1 activation segment. Blue residues were not mutated. The alanine scan has been performed with the mouse CLK1 kinase domain. Numbers of residues are shifted -1 compared to the human variant.

(B) *In vitro* kinase assay with CLK1 wt and mutants. Mutants S327A, E333A and Y344A were not expressible. All variants were purified from bacteria and coupled to glutathione beads, incubated with GST-SR and ^{32}P-γ-ATP at the indicated temperatures. After SDS-PAGE, phosphorylation was investigated by autoradiography (for each variant top, ^{32}P), equal loading was confirmed by Coomassie staining (bottom). For simplification only substrate phosphorylation of each variant is shown. Variants shifting the temperature optimum towards a higher temperature are boxed grey and brown, respectively.

(C) MD simulations confirm residue crucial for setting the inactivation temperature. Depicted are the distances between human CLK1 activation segment residue R343 (guanidinium group) and the γ phosphate of ATP (top), H344 (CE1) and ATP (2nd) and between R343 (CZ) and H344 (3rd) as observed in MD simulations at 20°C and 40°C. Additionally, distances between R343 and ATP in the CLK1 H344A mutant were investigated by MD simulations (bottom). Distances and probabilities are shown as mean +/- SD from three simulations. At 40°C we do not observe close R343-ATP proximity in the CLK1 H344A mutant as in the wt, suggesting that the H343 conformational change is instrumental to reposition R343 at higher temperature in the wt kinase.

(D-K) Superposition of CLK1 crystal structures and the structural models obtained by MD simulations at 20 and 40°C (average positions of the modelling). View into the active site. (D) Superposition of CLK1 bound to the 10Z-Hymenialdisine inhibitor (PDB ID 1Z57; CLK1 1Z57, shown in gray) and CLK1 bound to the ethyl 3-[(E)-2-amino-1-cyanoethenyl]-6,7-dichloro-1-methyl-1H-indole-2-carboxylate inhibitor (PDB ID 2VAG and 6TW2), adopting a double conformation. In one conformation, the activation segment points into the substrate binding groove (chartreuse), whereas in the second conformation (teal) it is practically indistinguishable from the canonical loop conformation (PDB ID 1Z57, shown in gray) that is interpreted as the active conformation. For clarity the inhibitors are not shown. (E) Superposition of CLK1-MD 20°C and CLK1-MD 40°C. (F, G) Structural model as obtained by MD simulations at 20°C (F, CLK1-MD 20°C) or at 40°C (G, CLK1-MD 40°C) in blue or red cartoon representation, the modelled ATP in stick representation, and Mg^{2+} as green sphere are shown. (H, I) Superposition of CLK1 1Z57 and either CLK1-MD 20°C (H) or CLK1-MD 40°C (I). (J, K) Superposition of CLK1 6TW2 and either CLK1-MD 20°C (J) or CLK1-MD 40°C (K).

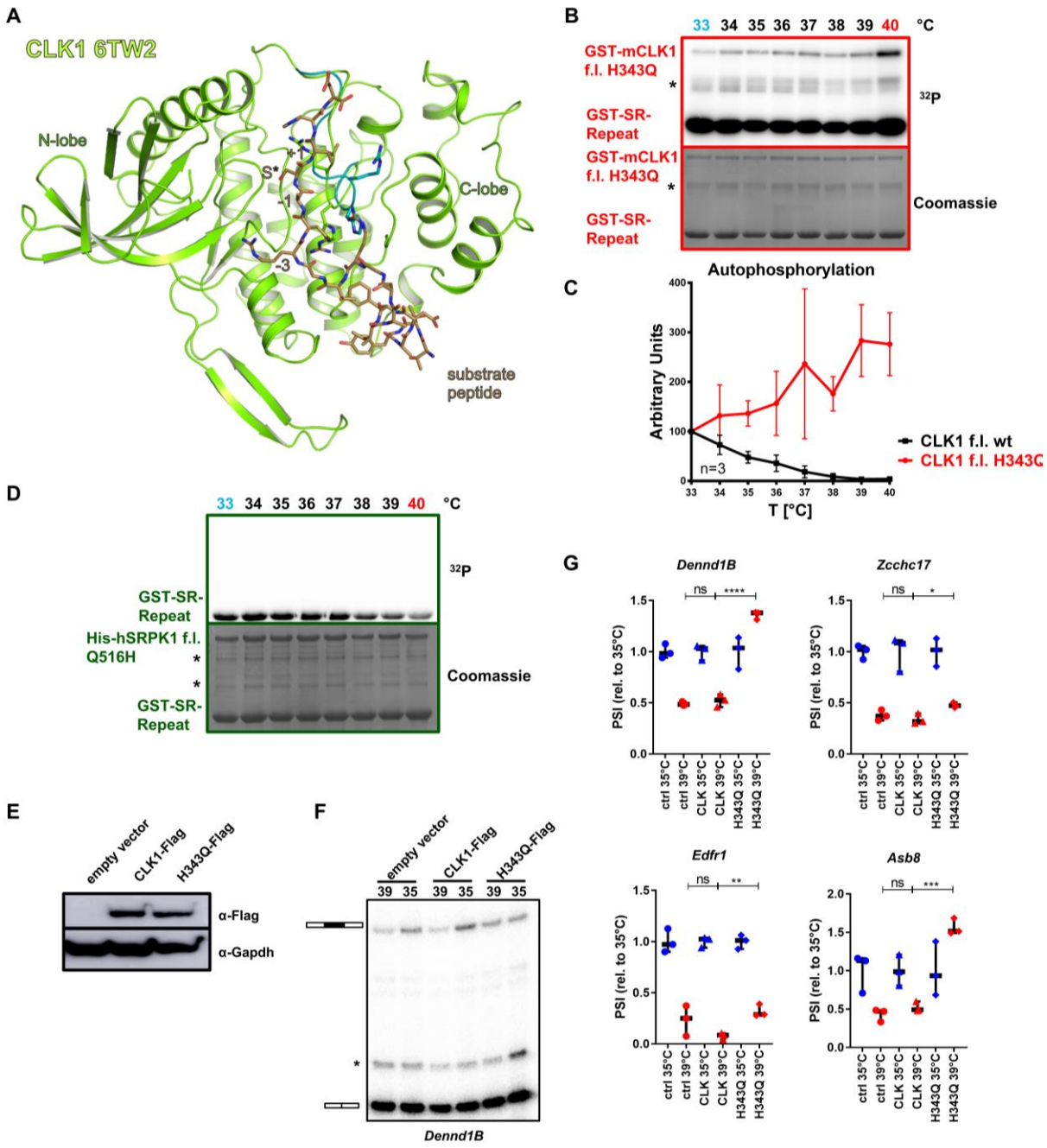

Figure S5. A single amino acid substitution renders CLK1 activity temperature insensitive (related to Figure 5)

(A) Superposition of the newly refined structure of CLK1 (PDB ID 6TW2), shown in cartoon representation, and the PKA substrate peptide (PDB ID 1JBP) to locate the potential binding site of a substrate peptide in CLK1. The substrate is shown in stick presentation and colored in light brown. In the newly refined structure of CLK1 the activation segment adopts a double conformation (residues T338 to R346). A double phosphorylation of S341/T342 induces a conformational change of the activation segment (colored in chartreuse) that in consequence rotates the side chains of both phosphorylated residues from an inside faced orientation to an outward faced conformation. In the second conformation the activation segment

adopts a conformation as observed in other crystal structures of CLK1 with an unphosphorylated activation segment (colored in teal). Residues in human CLK1 are shifted by +1 in comparison to the respective mouse residues.

(B) *In vitro* kinase assay with the f.l. CLK1 H343Q mutant. The mutant kinase was purified from bacteria and coupled to glutathione beads, incubated with GST-SR and ^{32}P-γ-ATP at the indicated physiological temperatures. After SDS-PAGE, phosphorylation was investigated by autoradiography (top, ^{32}P), equal loading was confirmed by Coomassie staining (bottom). The asterisks likely represent extended kinase domains, which lost the GST units due to cleavage in the unstructured N-termini by residual proteases and which are also not phosphorylated in a temperature-dependent manner.

(C) Quantification of auto-phosphorylation from experiments as in (B) relative to 33°C (n=3). Quantification of f.l. CLK1 wt from Figure 1. Data represent means +/- SD.

(D) *In vitro* kinase assay with f.l. SRPK Q516Has described in (B).

(E) Western Blot confirming similar levels of CLK1-Flag and H343Q-Flag overexpression, GAPDH served as loading control.

(F, G) Representative gel and quantification of splicing sensitive, radioactive RT-PCRs for targets shown in Figures 3E-F and S2E-F, in control cells, or in cells overexpressing CLK1-Flag (CLK1) or CLK1H343Q-Flag (H343Q). Shown is the fold change (PSI) relative to 35°C. Statistical significance was determined by unpaired t-tests. Note that we observe relatively more exon inclusion at 39°C when overexpressing the H343Q mutant (compared to overexpression of the WT) in all four examples. Note that *Dennd1B* and *Asb8* reveal even warm-induced exon inclusion upon H343Q overexpression (which could be explained by CLK4 activity leading to exclusion and CLK1 activity leading to inclusion of the exon; in this scenario the inclusion activity of CLK1 would still be present through the H343Q mutant, while the exclusion activity of CLK4 would be inactivated at 39°C). In contrast, Zcchc17 and Edfr1 are only mildly effected by overexpression of CLK1 H343Q, suggesting that both CLK1 and CLK4 activity leads to exon exclusion, probably through different SR proteins, with CLK4 playing a dominant role.

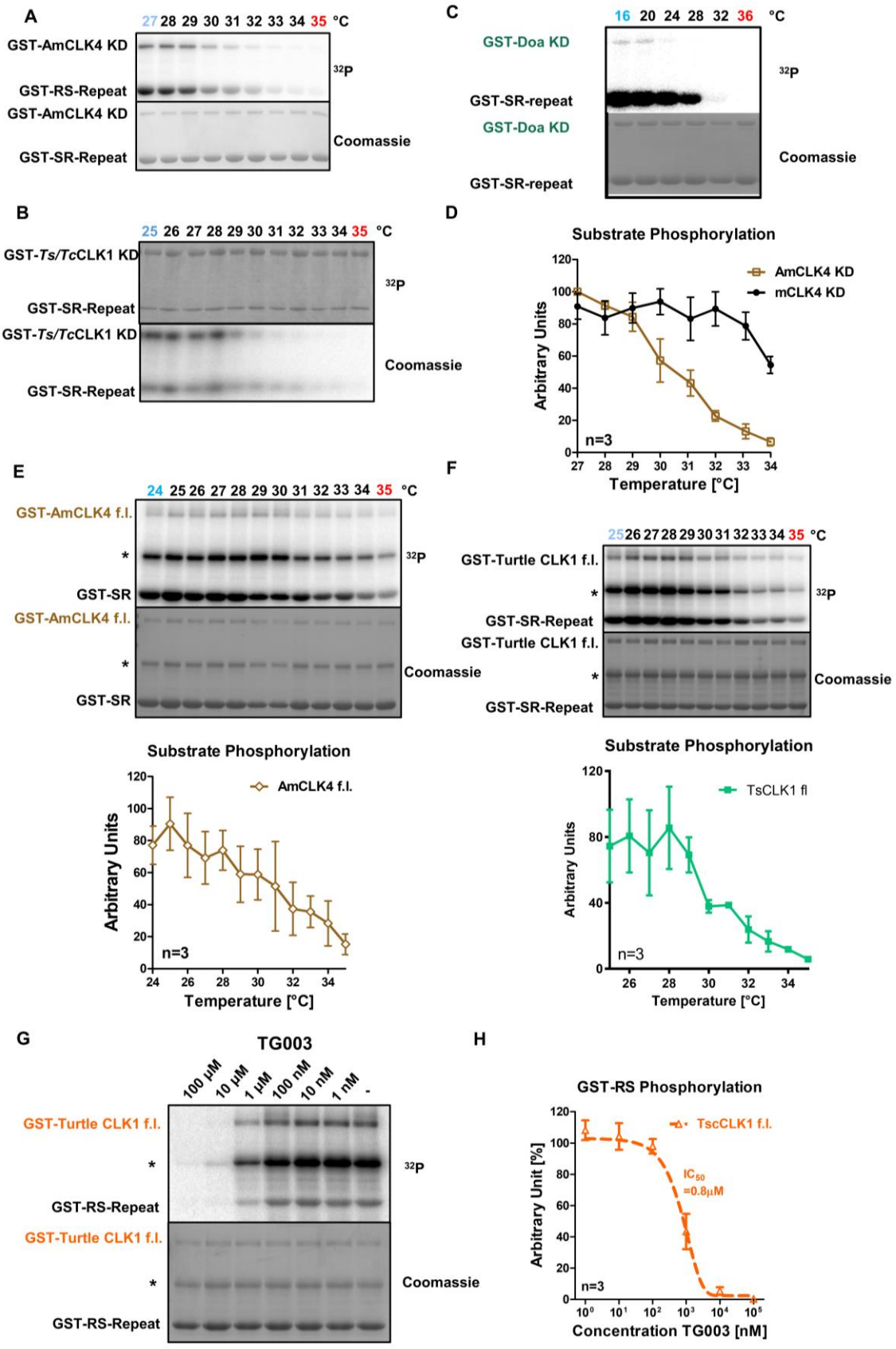

Figure legend on the next page

Figure S6. Temperature-dependent activity of poikilothermic CLK homologs is evolutionarily adapted (related to Figure 6)

(A-C) Representative gels of alligator (A), turtle (B) and fly (C) CLK homologs as in Figure 6B-D.

(D) Comparison of mouse (black) and alligator (brown) CLK4 kinase domain in the temperature range of alligator sex determination (n=3, mean +/- SD).

(E, F) Temperature-dependent activity of f.l. alligator CLK4 (E) and turtle CLK1 (F) in the sex determining temperature range. Below, quantification of f.l. CLK activity. Data represent mean +/- SD (n=3).

(G, H) f.l. turtle CLK1 is inhibited by the CLK inhibitor TG003 in a concentration range comparable to mammalian CLKs. Data in (H) represents mean +/- SD (n=3).